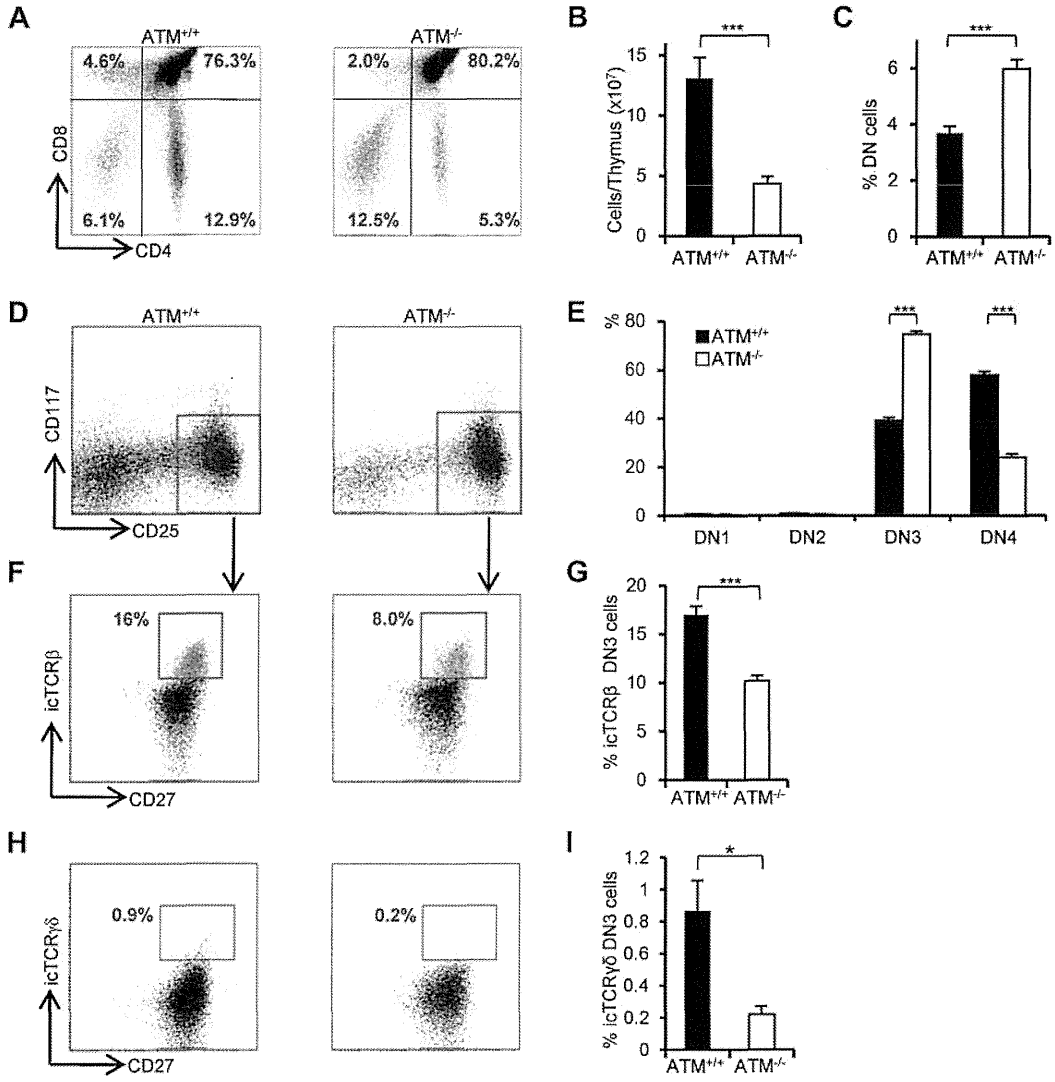

Figure 1. Developmental failure at the transition step from DN3a to DN3b in ATM$^{-/-}$ thymocytes. (A) Representative dot plots showing CD4 and CD8 profiles from ATM$^{+/+}$ and ATM$^{-/-}$ mice. (B) Absolute numbers of total thymocytes in ATM$^{+/+}$ and ATM$^{-/-}$ mice. (C) Relative percentage of lineage-negative cells. (D) Representative dot plots are gated on double-negative (DN) cells from ATM$^{+/+}$ and ATM$^{-/-}$ mice, when DN3 cells reached at 1 × 10^4 cells. Red dots indicate DN3b cells that are back-gated from CD27$^+$icTCR-β$^+$ fraction. (E) Bar graph represents DN1, DN2, DN3, and DN4 thymocyte percentages. (F) Dot plots are gated on DN3 cells (CD25 low, indicated in red in the top panels). DN3a cells are shown as CD27^{low} intracellular (ic) TCR-β$^-$. DN3b cells are CD27^{high}icTCR-β$^+$ and are indicated as red dots in red squares. (G) Bar graph represents icTCR-β–positive DN3b thymocyte percentages in the DN3 fraction. (A-G) The data were obtained from 12 ATM$^{+/+}$ mice and 11 ATM$^{-/-}$ mice at 4 to 8 weeks of age. (H) Dot plot data gated on DN3 cells from ATM$^{+/+}$ and ATM$^{-/-}$ mice. The icTCR-γδ–positive cells, which are indicated as red dots in the black squares, are CD27$^+$icTCR-γδ$^+$. (I) Percentages of icTCR-γδ–positive DN3b thymocytes in the DN3 fraction. (H-I) Data were obtained from 6 ATM$^{+/+}$ mice and 5 ATM$^{-/-}$ mice. Data are representative of at least 3 independent experiments (mean ± SE). *$P < .05$, ***$P < .001$.

(supplemental Figure 5B-C). We further examined the expression profiles of genes essential for early T-cell development, such as BCL11b, pTα, RAG1, and RAG2, in ATM$^{-/-}$ mouse thymocytes and found that they were normally expressed (supplemental Figure 6). These results indicate that the impaired development seen at the DN stage of ATM$^{-/-}$ thymocytes is not the result of the failure of the pre-TCR complex-dependent signaling pathway.

ATM-deficient thymic stroma supports normal transition from DN3a to DN3b

ATM-deficient thymic stromal cells reportedly do not affect the transition failure from DP to SP phase using BMT experiments.[30] Recent reports have identified a role for the stromal cell derived factor 1α and its receptor CXC chemokine receptor 4 in β-selection.[31,32] The functional role of ATM-deficient thymic stromal cells in β-selection of thymocytes has not been fully elucidated. To determine whether ATM-deficient thymic stromal cells affect thymocyte differentiation during DN phase, BM from ATM$^{+/+}$ and ATM$^{-/-}$ C57/BL6 Ly5.2 donors was transplanted into lethally irradiated wild-type ATM$^{+/+}$ C57/BL6 Ly5.1 recipients. Consistent with the result observed in ATM$^{-/-}$ mice, total thymocyte cellularity and absolute number of TCR-β and TCR-γδ T cells gated on CD45.2 were significantly reduced in the ATM$^{-/-}$ donor group (Figure 4A-C). ATM$^{-/-}$ thymocytes (CD45.2) in vivo reconstituted in the wild-type thymus also showed the transitional failure from DN3a to DN3b phase (Figure 4D-F). These findings of in vivo ATM$^{-/-}$ thymocyte differentiation in the thymic environment of ATM$^{+/+}$ C57/BL6 Ly5.1 corresponded well to the findings in those cultured on OP9-DLL1 in vitro (Figure 2E-F). These results ruled out the possibility that differentiation defect of thymocytes at β-selection checkpoint is caused by thymic environment in the absence of ATM.

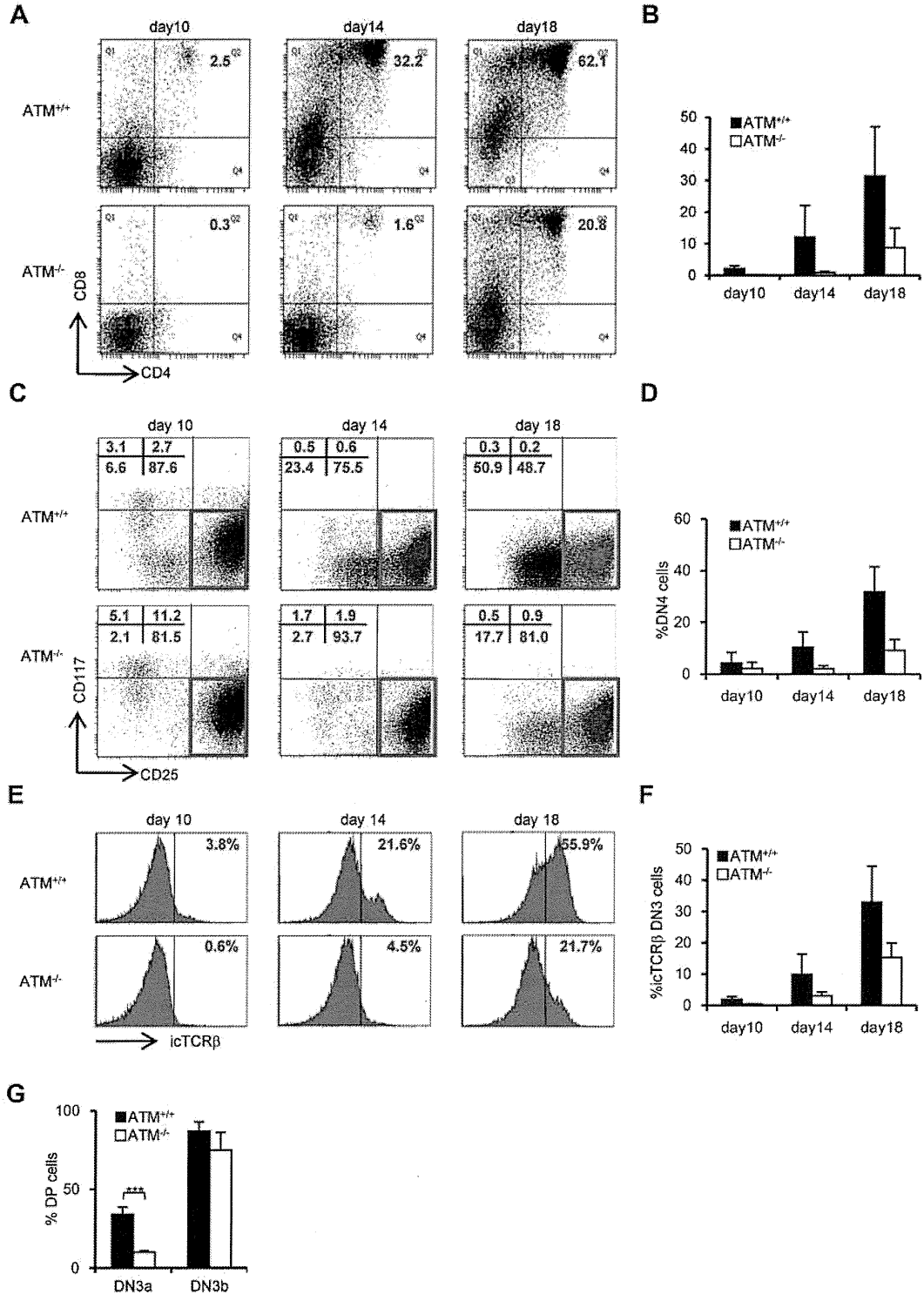

Figure 2. Transition failure from DN3a to DN3b is recapitulated in in vitro culture. Bone marrow progenitors (1×10^4 cells) from 4- to 8-week-old adult BM were cultured with OP9-DLL1 cells supplemented with 5 ng/mL of Flt3L and 1 ng/mL of IL-7 for 18 days. Differentiated cells were harvested on the indicated days. (A) Representative dot plots showing the surface expression of CD4 and CD8 (top) from $ATM^{+/+}$ and $ATM^{-/-}$ BM progenitors. (B) Percentages of $CD4^+CD8^+$ DP phase cells at the indicated time points. (C) Dot plots are gated on DN phase from $ATM^{+/+}$ and $ATM^{-/-}$ BM progenitors. Red squares represent DN3 cells. Representative dot plots are shown when DN3 cells reached 1×10^4 cells. Red dots indicate DN3b cells that are back-gated from the $CD27^+$icTCR-β^+ fraction. (D) Percentages of DN4 phase at the indicated time points. (E) Representative histograms showing expression of icTCR-β on DN3 cells. (F) Percentages of icTCR-β–positive cells on DN3 cells at the indicated time points. Data are representative of 3 independent experiments. Bar graphs represent mean ± SE. (G) Singly sorted DN3a and DN3b cells from each $ATM^{+/+}$ and $ATM^{-/-}$ thymus were cultured on OP9-DLL1. Percentage of cells successfully differentiated to $CD4^+$ and $CD8^+$ (DP) phase were evaluated by flow cytometry on day 4. Bar graph represents mean percentage from 5 independent experiments. Data are mean ± SE. ***$P < .001$.

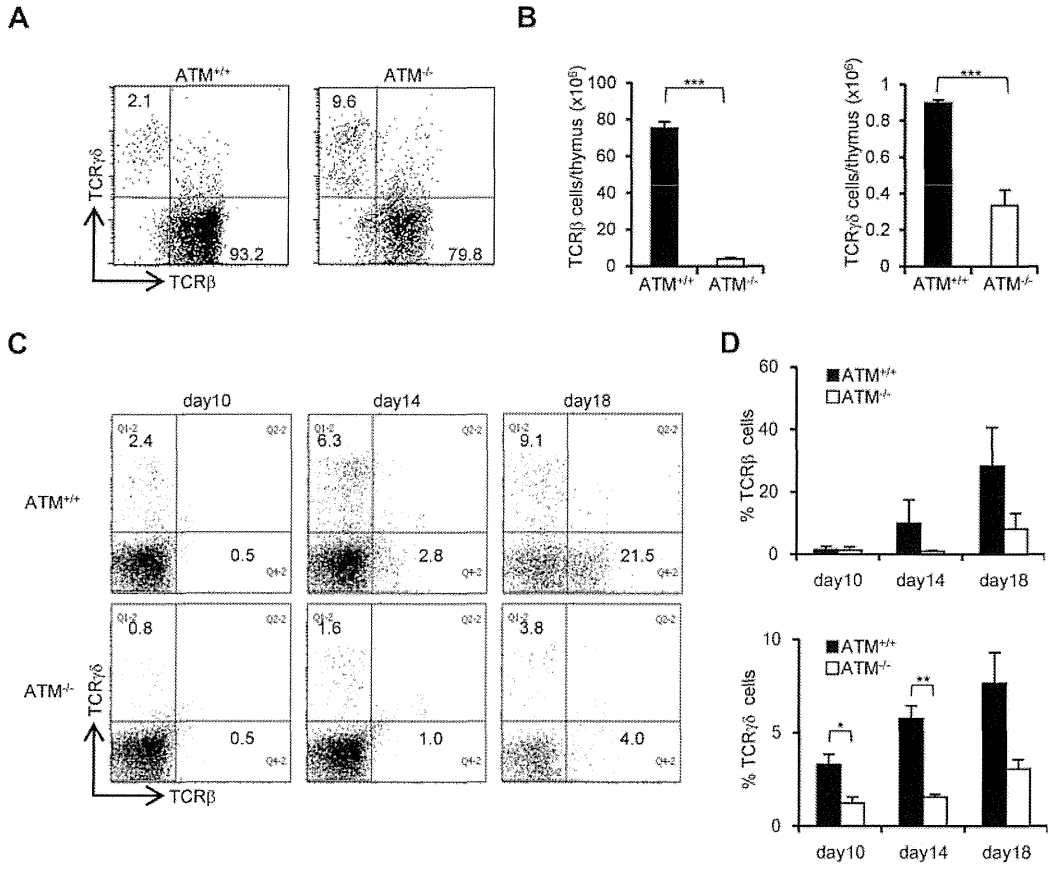

Figure 3. Both αβ and γδ T-cell developments are impaired in the ATM$^{-/-}$ thymus. (A) Dot plots for TCR-β and TCR-γδ expression gated on CD3-positive cells from ATM$^{+/+}$ and ATM$^{-/-}$ thymi. Data are representative of 3 independent experiments. (B) Absolute numbers of TCR-β (left) and TCR-γδ (right)–positive T cells from ATM$^{+/+}$ (n = 4) and ATM$^{-/-}$ (n = 6) thymi. Data are mean ± SE. ***$P < .001$. (C) BM progenitors were cultured with OP9-DLL1 cells supplemented with 5 ng/mL of Flt3L and 1 ng/mL of IL-7 for 18 days. Differentiated cells were harvested on indicated days and stained for surface TCR-β and TCR-γδ. Dot plots are gated on CD45-positive cells from ATM$^{+/+}$ and ATM$^{-/-}$ BM progenitors at the indicated time points. Data are representative of 3 independent experiments. (D) Percentages of TCR-β and TCR-γδ-positive cells at the indicated time points. Data are mean ± SE. *$P < .05$. **$P < .01$.

Nonequivalent TCR-β recombination and an increase in DNA DSBs in ATM$^{-/-}$ thymocytes

It has been shown that ATM$^{+/+}$ and ATM$^{-/-}$ DN thymocytes have nearly equivalent levels of Jδ and Jβ1 signal end joining; however, there are reportedly higher levels of unrepaired Jβ1.1, Jβ1.2, and Jδ1 coding ends in ATM$^{-/-}$ mice.[15] PCR analysis of TCR Dβ1-J1, Dβ2-J2, Vβ1-J1, Vβ4-J1, Vβ8-J1, Vβ1-J2, Vβ4-J2, and Vβ8-J2 recombination in DN2, DN3a, DN3b, and DP stage cells showed almost the same extent of polyclonal rearrangement in ATM$^{+/+}$ and ATM$^{-/-}$ mice (Figure 5A; supplemental Figure 7A-B). However, the Vβ12-J1, Vβ15-J1, Vβ16-J1, Vβ12-J2, Vβ15-J2, and Vβ16-J2 rearrangements were relatively reduced in ATM$^{-/-}$ thymocytes (Figure 5A; supplemental Figure 7B), which is identical to that in thymocytes of mice engineered to express only the RAG2 core protein.[33] Then, we speculated that DSBs at TCR-γ, -δ, and -β loci would remain unresolved in DN3a stage thymocytes of ATM$^{-/-}$ mice. Correspondingly, the frequency of γH2AX-positive cells, a marker for DSBs, was analyzed and shown to be higher in DN2 and DN3 and persist until DP in ATM$^{-/-}$ mice (Figure 5B).

ATM-deficient DN3a cells are defective in cell-cycle regulation and prone to apoptosis

The in vivo cell-cycle profile and level of apoptosis induction were also investigated. Stringent regulation of the timing of gene recombination is crucial for maintaining genomic integrity during normal lymphocyte development. RAG-mediated recombination is limited to the noncycling (G_1) phase of the cell cycle; cells preferentially arrest at G_1 and undergo RAG-mediated TCR-γ, -δ, or -β recombination in the DN3a stage. Cells that successfully achieved normal TCR-γ, -δ, or -β recombination resume cell-cycle progression toward DN3b. Another wave of transient cell-cycle arrest occurs in the early DP phase when the TCR-α locus begins to recombine. Although the cell-cycle profiles of thymocytes in ATM$^{+/+}$ and ATM$^{-/-}$ were not significantly different from one another in the DN2 stage, more ATM$^{-/-}$ cells than ATM$^{+/+}$ cells were observed to be cycling through DN3a into the DP phases (Figure 5C). Furthermore, apoptotic cells were significantly increased in DN3a cells from ATM$^{-/-}$ mice (Figure 5D), corresponding to the previous findings that thymocytes that fail to functionally rearrange the TCR-β chain undergo apoptosis.

Chromosomal breaks at the TCR-α/δ locus and translocations in T-cell progenitors lacking ATM

ATM$^{-/-}$ lymphocytes and leukemia/lymphoma cells exhibit characteristic intralocus rearrangements involving either the TCR or IGH locus.[17,34-36] Chromosomal translocations with gene amplification involving the TCR-α/δ locus were also observed in ATM-deficient mice.[17,37] Based on our findings, we hypothesized that the DN3a to DN3b transition, which is defective in ATM$^{-/-}$ thymocytes, is the window with the highest risk for the formation of

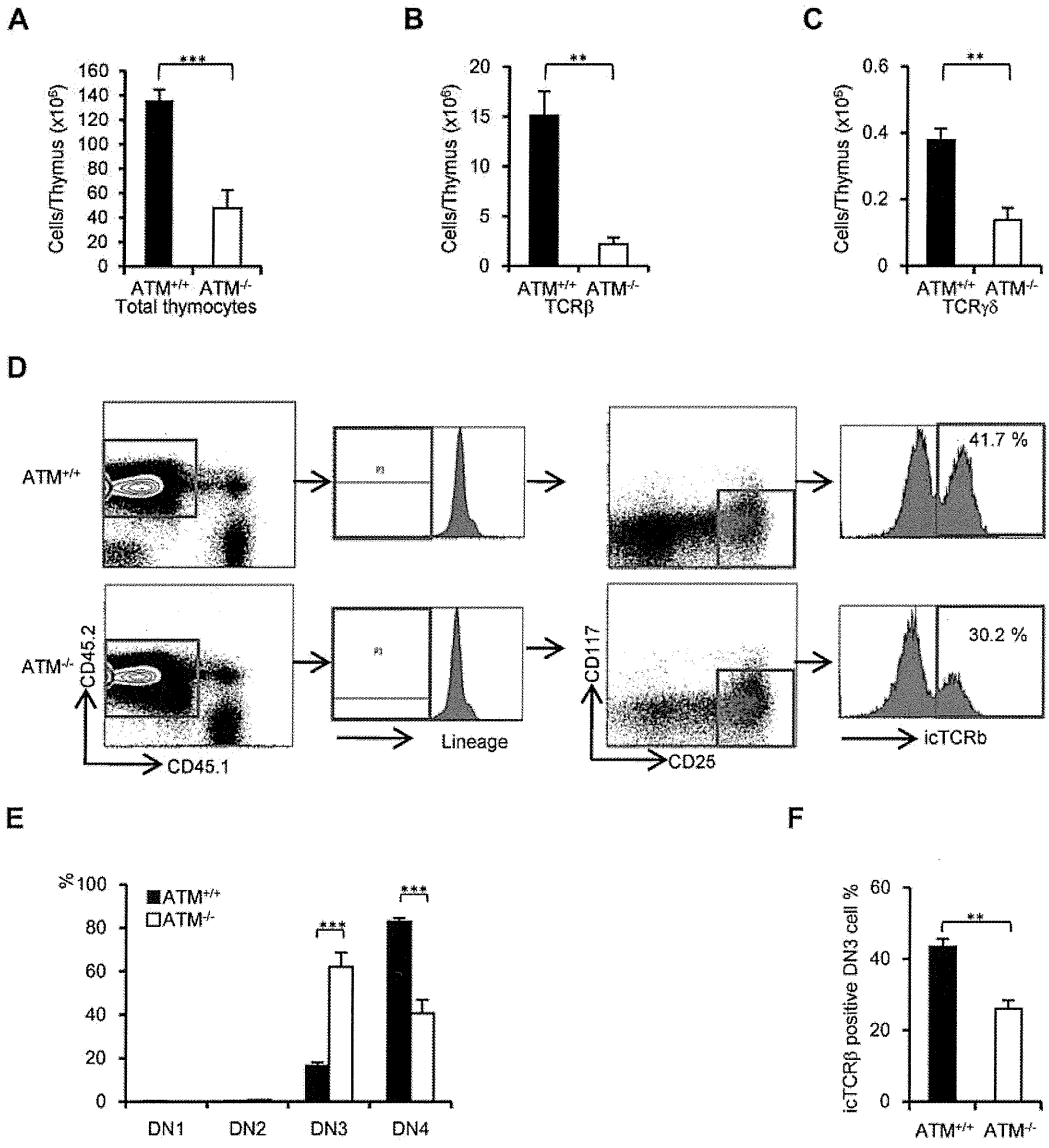

Figure 4. Thymic stromal cells of ATM$^{-/-}$ mice support DN3a to DN3b transition normally. Bone marrow cells from ATM$^{+/+}$ or ATM$^{-/-}$ mice (Ly5.2) were transferred into lethally irradiated ATM$^{+/+}$ mice (Ly5.1). The thymi were harvested from the reconstituted recipient ATM$^{+/+}$ (Ly5.1) mice at 4 weeks after BMT. (A-C) Total thymocytes, TCR-β–positive cells, and TCR-γδ–positive cells were calculated on CD45.2-positive cells. For each group, more than 3 mice were analyzed. (D) Flow cytometric data from ATM$^{+/+}$ thymocytes (Ly5.1) reconstituted with ATM$^{+/+}$ or ATM$^{-/-}$ BM progenitors (Ly5.2). Cells were gated on CD45.2-positive and lineage-negative fractions and analyzed for CD25 and CD117 marker expression. Histograms show icTCR-β positivity in the DN3 phase. DN3b cells as defined by icTCR-β positivity were back-gated to the DN3 fraction and are indicated as red dots. Data are representative of 3 independent experiments. (E) Percentages of DN1, DN2, DN3, and DN4 cells in ATM$^{+/+}$ (Ly5.1) recipient mice that received either ATM$^{+/+}$ or ATM$^{-/-}$ BM progenitors (Ly5.2). Cells were gated on CD45.2 and analyzed. (F) Percentages of icTCR-β–positive DN3b thymocytes in the DN3 fraction in ATM$^{+/+}$ (Ly5.1) recipient mice transplanted and gated as in panel E are shown. Data are mean ± SE. $^{**}P < .01$, $^{***}P < .001$.

chromosome 14 translocations involving TCR-α/δ locus breaks. To monitor chromosome 14 integrity before and after the DN3a phase, an in vitro coculture system, which has been developed by modifying a previously reported system,[38] combined with FISH analysis was performed (supplemental Figure 8). Normal chromosome 14, as shown in red, contains colocalized blue and green foci corresponding to the 5′- and 3′-end of the TCR-α/δ loci, respectively (Figure 6A). Chromosome 14 breaks at the TCR-α/δ locus were observed in 5% of ATM$^{-/-}$ DN2/DN3a cells (54 of 1073 metaphase cells) and 2.5% of ATM$^{-/-}$ DN3b/DN4 cells (11 of 437 metaphase cells; Figure 6B; supplemental Tables 1 and 2), but none in the ATM$^{+/+}$, ATM$^{+/-}$RAG2$^{-/-}$, or ATM$^{-/-}$RAG2$^{-/-}$ cells, indicating that these breaks in ATM$^{-/-}$ thymocytes are RAG-dependent. Chromosome 14 translocations involving the TCR-α/δ locus were occasionally detected in ATM$^{-/-}$ DN2/DN3a cells (1.77%; 19 of 1073 metaphase cells), but not in ATM$^{+/+}$ (961 metaphase cells), ATM$^{+/-}$RAG2$^{-/-}$ (985 metaphase cells), or ATM$^{-/-}$RAG2$^{-/-}$ cells (1034 metaphase cells). Interestingly, the frequency of these chromosomal translocations dramatically increased during the progression to DN3b/DN4 in ATM$^{-/-}$ cell (11.4%; 50 of 437 metaphase cells; Figure 6C; supplemental Tables 1-2). These results suggest that chromosome 14 translocations involving TCR-α/δ locus are mainly generated during DN3a to DN3b transitional stage.

Interestingly, some of the dicentric chromosome 14s carried amplification upstream of the TCRV-α locus (Figure 6D-E), an abnormality that is frequently observed in ATM$^{-/-}$ thymic lymphoma cells (supplemental Figure 9). In this culture system, the

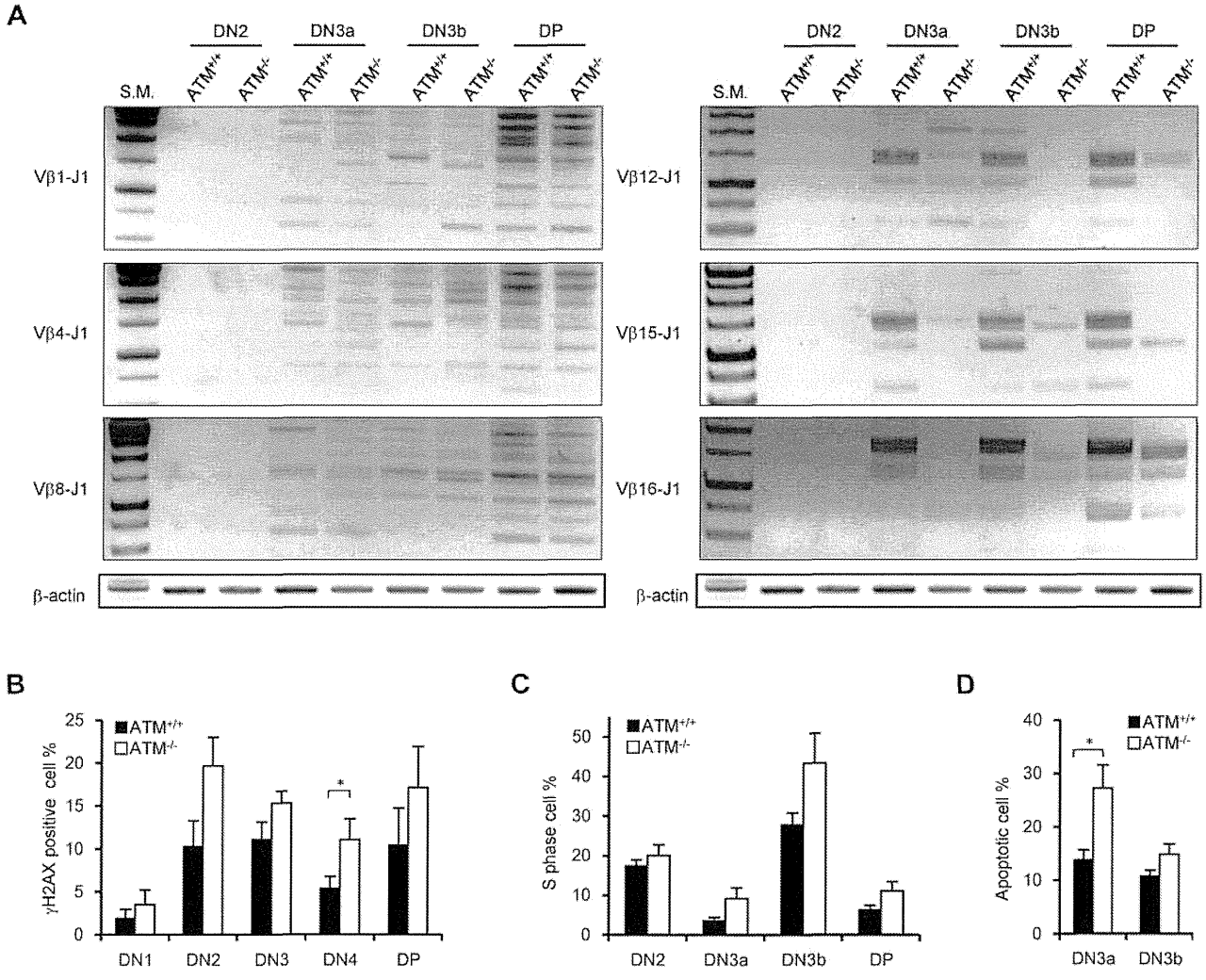

Figure 5. Nonequivalent TCR-β recombination and an increase in DNA DSBs in ATM$^{-/-}$ thymocytes. (A) Rearrangement status of TCR Vβ1-Jβ1, Vβ4-Jβ1, Vβ8-Jβ1,Vβ12-Jβ1, Vβ15-Jβ1, and Vβ16-Jβ1 in the DN2, DN3a, DN3b, and DP stages was analyzed by PCR. (B) γH2AX-positive cell percentages in the DN1 to DP phases by flow cytometry. (C) Percentage of cells in S phase determined by flow cytometric analysis for PI and EdU incorporation at the DN2 to DP stages in ATM$^{+/+}$ (n = 3)and ATM$^{-/-}$ thymocytes (n = 4). (D) Apoptotic cell percentages determined by flow cytometric analysis for annexin V positivity in the DN3a and DN3b stages. Data are mean ± SE. *$P < .05$.

other characteristic abnormalities, including aneuploidy, were also identified during the DN2/DN3a and DN3b/DN4 stages (Figure 6D-E; supplemental Table 3). Sister chromatid breaks in chromosome 12 during mitotic phase and subsequent t(12;14) translocations were also observed in a minor fraction of cells at the DN2/DN3a and DN3b/DN4 stages (Figure 6E; supplemental Figure 10). Chromosome 12, which contains the IGH and BCL11b loci, is often a reciprocal chromosome 14 translocation partner in ATM-deficient thymic lymphoma.

Discussion

In this study, we have visualized, for the first time, the critical developmental step of TCR-α/δ chromosomal breaks and translocations in ATM-deficient thymocytes and narrowed down the DN3a to DN3b stages to be the window for these events.

DN phase differentiation failure in ATM-deficient thymocytes has been speculated to be the result of faulty V(D)J recombination by in vitro studies.[14] Transition failure from DP to SP phase was also reported in in vivo thymus.[8,9] However, accurate profiles for T-cell development at DN phase have not been elucidated in ATM-deficient thymocytes. In addition, some other possibilities need to be ruled out that ATM-deficient thymic stromal cell has negative effect for DN phase development, and ATM itself has roles for a differentiation program, such as transcription factor and signal mediator. We find that DN3a and DN3b differentiation failure is only the result of TCR recombination failure, but not defective thymic stromal cells or aberrant differentiation program in ATM-deficient thymocytes. In the absence of ATM, DN2/DN3a thymocytes were demonstrated to be defective in TCR-γδ and TCR-β recombination, as evidenced by a failure of intracellular TCR-γδ and β expression. They were defective in differentiation toward both αβ and γδ-T-cell lineage in vitro, and absolute numbers of αβ and γδ T cells were decreased in ATM$^{-/-}$ thymus. These findings suggest that T-lymphopenia in ATM-deficient mice is caused by differentiation failure of thymocytes at the early stage from DN3a to DN3b before the stage from DP to SP by defective resolution of TCR breaks.

We demonstrated that the recombinations of TCR Vβ12, Vβ15, and Vβ16-DJ were not successful in ATM$^{-/-}$ thymocytes compared with those of Vβ1, Vβ4, and Vβ8-DJ (Figure 5A). This

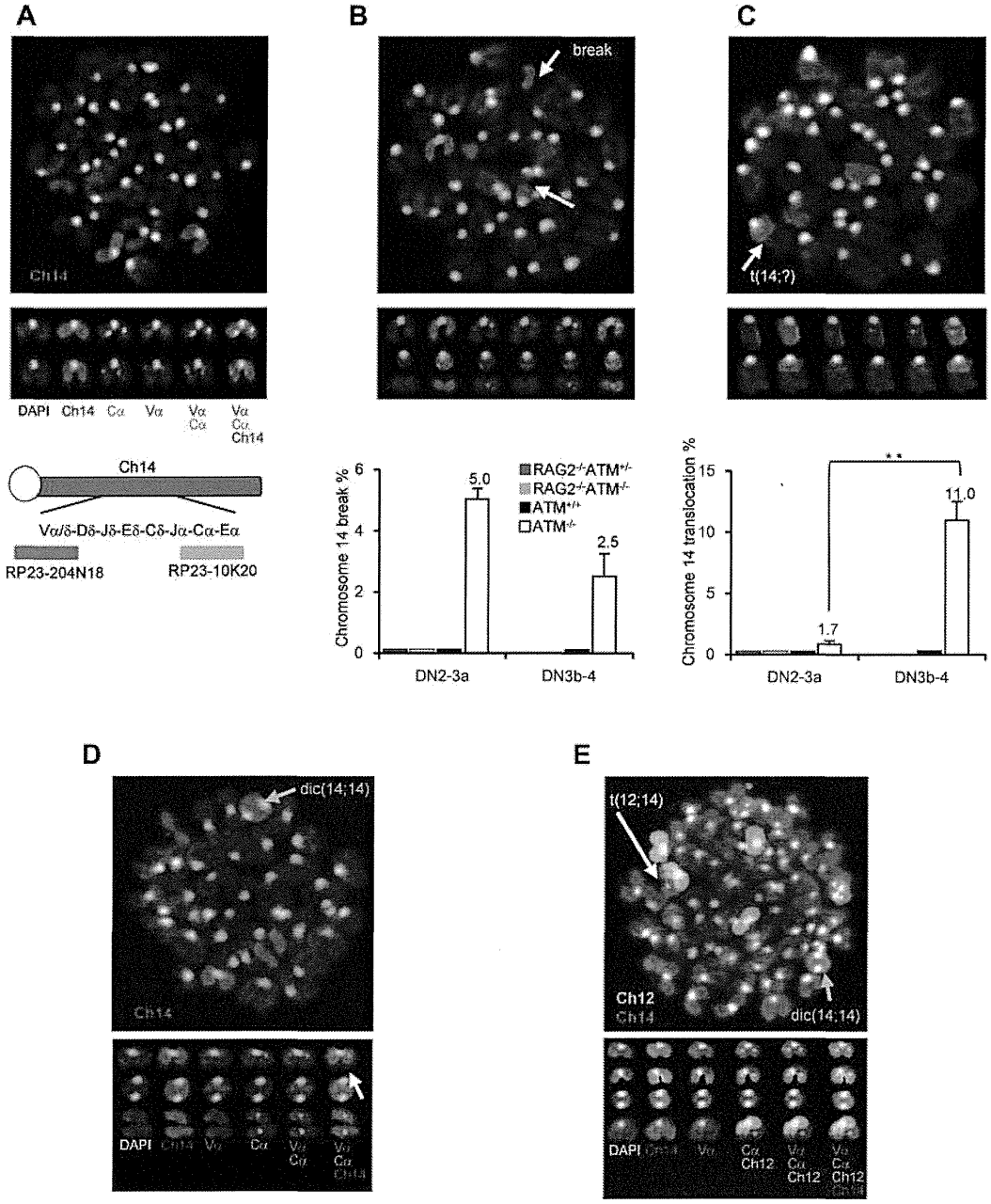

Figure 6. Chromosomal breaks at the TCR-αδ locus and translocations in T-cell progenitors lacking ATM. (A) Normal karyotype; FISH probe hybridized with 5′-TCR-α/δ (blue) and 3′-TCR-α/δ (green). Red represents the chromosomal paint probe for mouse chromosome 14. E indicates defined transcriptional enhancer elements. (B) Representative images of breaks between 5′TCR-α/δ (blue) and 3′TCR-α/δ (green) on chromosome 14 (red; top panel). The percentage of DN2/DN3a cells and DN3b-DN4 cells with a TCR-α/δ locus break is shown in a bar graph (bottom panel). Thymocyte maturation arrests at the DN2/DN3a stage in RAG2$^{-/-}$ mice; thus, DN3b-DN4 phase locus breaks cannot be measured. (C) Representative images of a chromosomal translocations (top panel). The percentage of cells with a chromosome 14 translocations is shown in a bar graph (bottom panel). y-axis indicates change to percentage chromosome 14 breaks and translocations. (D) Representative images of chromosomal abnormalities showing the TCR-α/δ locus on a dicentric chromosome 14 (yellow arrow) and breaks (white arrow). (E) Representative image of a chromosomal 12;14 translocation (white arrow) and a dicentric chromosome 14 (yellow arrow). Data are mean ± SE. $^{**}P < .01$.

skewed pattern of TCR-β recombination is identical to that in thymocytes of mice engineered to express only the RAG2 core protein (Rag2$^{c/c}$; ie, the portion of the molecule that, together with core RAG1, is the minimal region required for in vitro V(D)J recombination). RAG2$^{c/c}$ mice show inefficient recombination for Vβ10, Vβ11, Vβ12, and Vβ15 compared with Vb2 and Vb8 because of a different RSS spacer sequence in these groups.[33] Our findings and these observations seen in the Rag2$^{c/c}$ mouse suggest that ATM and RAG protein might interact or ATM may modify RAG function by phosphorylation or not during recognition of specific RSS sequence for V(D)J recombination. Furthermore, Rag2$^{c/c}$p53$^{-/-}$ mice exhibit similar phenotype with ATM-deficient DN profiles and rapidly develop lymphoma with chromosome translocations at the TCR-δ locus.[37] The defects of T-cell development in these engineered mice are mainly the result of the loss of interaction between the RAG postcleavage complex with ATM and is compatible with our observation in ATM$^{-/-}$ thymocytes.

RAG1 is expressed throughout the cell cycle, whereas RAG2 is periodically destructed at the G_1-to-S transition and is stable only during G_0 or G_1 phase, which limits V(D)J recombination to occur only at G_0 and G_1 cell-cycle phases. Thus, coordinated RAG expression and organized cell-cycle checkpoint are indispensable

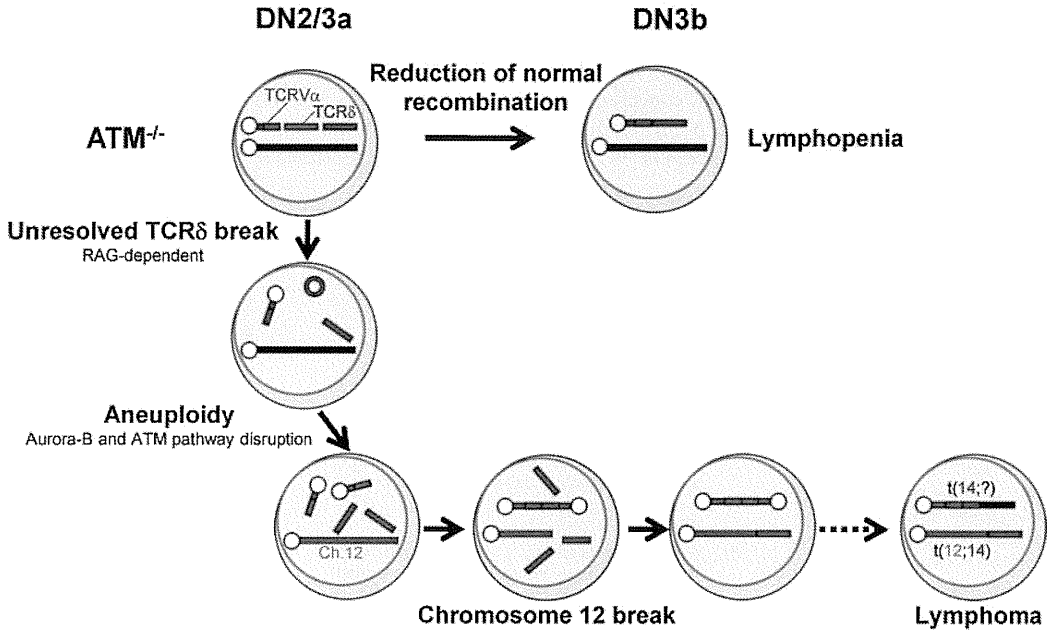

Figure 7. Model for thymocyte development lacking ATM. Schematic illustration for the impaired thymocyte development and creation of a translocation involving the TCR locus.

to prevent aberrant chromosome translocation.[11,39] Cell-cycle deregulation to enter S-phase was observed in phases through DN2 to DP in ATM$^{-/-}$ thymocytes. Thus, it is probable that the G_1-S checkpoint failed to be activated in ATM$^{-/-}$ thymocytes possibly involving or not the failure of Pim2 kinase expression that is mediated by ATM.[40] In our analysis, it was also noted that apoptotic cells were significantly increased in DN3a in ATM$^{-/-}$ thymocytes. Together, these findings unresolved coding end joining concomitant with disorganized cell-cycle checkpoint regulation as well as increased DNA breaks associated with apoptotic nuclear events might lead to genomic instability in early developmental stages of T cells in ATM$^{-/-}$ mice.[41,42]

Our findings led us to propose the following model for the process of generation of chromosome breaks and translocations in ATM deficiency. During DN2/DN3a, RAG-mediated breaks are generated, and they persist beyond the G_1 phase because of defective TCR-β V-DJ recombination and cell-cycle progression. These cells are detected as those carrying chromosomal breaks at TCR-δ on chromosome 14 (Figure 6B). After the DN3b stage, some of these chromosomes recombine with unknown partner chromosomes or occasionally with an inappropriately replicated chromosome 14 itself, leading to dicentric chromosome formation. Occasionally, the upstream TCRV-α locus is amplified by multiple cycles of this process (Figure 6D-E). These findings are reflected by those that aurora-B mediated mitotic ATM activation and the spindle checkpoint play essential roles to suppress aneuploidy.[43] Genomic instability associated with ATM deficiency may also generate chromatid breaks, including chromosome 12, which were observed in minor fraction compared with RAG-dependent chromosome 14 breaks (supplemental Figure 10). Chromosome 12 is a well-known partner of chromosome 14 translocation in ATM$^{-/-}$ thymic lymphoma. The break sites on chromosome 12 are widely spread on 30-Mb-long from IGH locus to centromeric portion involving BCL11b and TCL1 loci, not always involving cryptic RSS,[17] and breaks were detected as chromatid breaks, not as bilateral chromosomal breaks. Taken together, these findings suggest that chromosome 12 breaks presumably occur in RAG-independent manner after completion of sister chromatid synthesis.

These processes, be they random or nonrandom, may lead to chromosome translocations, some of which may somehow get through the checkpoints by successful TCR-γδ or TCR-β recombination and lead to the development of phenotypically normal lymphocytes, yet carrying over oncogenic potentials, after the DN3b/DN4 stages. Loss of genomic guardian systems, such as the ATM-p53 pathway, may enhance additional steps for tumorigenesis.[44] Together with these findings, the initial step of multistep evolutions toward lymphomagenesis was visualized in ATM-deficient thymocytes. RAG-dependent failure during TCR recombination and RAG-independent disruption of chromosomal architecture may be intimately involved in the process for tumor formation.

In conclusion, T-cell developmental failure leading to immunodeficiency and chromosomal translocations involving the TCR-α/δ locus derive from mutually integrated events during the DN2/DN3a stages in ATM-deficient T cells (Figure 7). We propose that our in vitro experimental method is also useful for the functional validation of mutation-targeted therapeutic technologies for AT patients in the future.[45] In light of the finding that 35% of T-cell acute lymphoblastic leukemias carry chromosomal translocations involving *TCR* genes,[46] our findings also suggest that epigenetic dysregulation of ATM or posttranscriptional deregulation of *ATM* gene might be involved in the formation of chromosomal translocations involving *TCR* genes in some T-cell leukemias with an apparently normal *ATM* gene.

Acknowledgments

The authors thank P. J. McKinnon for providing ATM$^{+/-}$ mice; M. F. Greaves, P. D. Burrows, and K. Enomoto for critical reading for manuscript; and Y. Kutami for technical support.

This work was supported by a Grant-in-Aid from the Ministry of Education, Science, and Culture (Japan) and Grant-in-Aid from the Ministry of Health, Labor and Welfare (Japan; M.T. and S.M.).

Authorship

Contribution: T. Isoda, M.T., T.M., H.K., and S.M. conceived the study and wrote the paper; and T. Isoda, J.P., S.N., M.S., K.M., T. Ikawa, and M.A. designed and performed experiments.

Conflict-of-interest disclosure: The authors declare no competing financial interests.

Correspondence: Masatoshi Takagi and Shuki Mizutani, Department of Paediatrics and Developmental Biology, Tokyo Medical and Dental University, 1-5-45 Bunkyo-ku, Yushima, Tokyo 113-8519, Japan; e-mail: m.takagi.ped@tmd.ac.jp or smizutani.ped@tmd.ac.jp.

References

1. Shiloh Y. ATM and related protein kinases: safeguarding genome integrity. *Nat Rev Cancer.* 2003;3(3):155-168.
2. Bakkenist CJ, Kastan MB. Initiating cellular stress responses. *Cell.* 2004;118(1):9-17.
3. Kastan MB, Bartek J. Cell-cycle checkpoints and cancer. *Nature.* 2004;432(7015):316-323.
4. Lavin MF. Ataxia-telangiectasia: from a rare disorder to a paradigm for cell signalling and cancer. *Nat Rev Mol Cell Biol.* 2008;9(10):759-769.
5. Nowak-Wegrzyn A, Crawford TO, Winkelstein JA, Carson KA, Lederman HM. Immunodeficiency and infections in ataxia-telangiectasia. *J Pediatr.* 2004;144(4):505-511.
6. Morio T, Takahashi N, Watanabe F, et al. Phenotypic variations between affected siblings with ataxia-telangiectasia: ataxia-telangiectasia in Japan. *Int J Hematol.* 2009;90(4):455-462.
7. Barlow C, Hirotsune S, Paylor R, et al. Atm-deficient mice: a paradigm of ataxia telangiectasia. *Cell.* 1996;86(1):159-171.
8. Matei IR, Gladdy RA, Nutter LM, Canty A, Guidos CJ, Danska JS. ATM deficiency disrupts Tcra locus integrity and the maturation of CD4+CD8+ thymocytes. *Blood.* 2007;109(5):1887-1896.
9. Vacchio MS, Olaru A, Livak F, Hodes RJ. ATM deficiency impairs thymocyte maturation because of defective resolution of T cell receptor alpha locus coding end breaks. *Proc Natl Acad Sci U S A.* 2007;104(15):6323-6328.
10. Bhatti S, Kozlov S, Farooqi AA, Naqi A, Lavin M, Khanna KK. ATM protein kinase: the linchpin of cellular defenses to stress. *Cell Mol Life Sci.* 2011;68(18):2977-3006.
11. Schatz DG, Ji Y. Recombination centres and the orchestration of V(D)J recombination. *Nat Rev Immunol.* 2011;11(4):251-263.
12. Perkins EJ, Nair A, Cowley DO, Van Dyke T, Chang Y, Ramsden DA. Sensing of intermediates in V(D)J recombination by ATM. *Genes Dev.* 2002;16(2):159-164.
13. Gostissa M, Alt FW, Chiarle R. Mechanisms that promote and suppress chromosomal translocations in lymphocytes. *Annu Rev Immunol.* 2011;29:319-350.
14. Bredemeyer AL, Sharma GG, Huang CY, et al. ATM stabilizes DNA double-strand-break complexes during V(D)J recombination. *Nature.* 2006;442(7101):466-470.
15. Huang CY, Sharma GG, Walker LM, Bassing CH, Pandita TK, Sleckman BP. Defects in coding joint formation in vivo in developing ATM-deficient B and T lymphocytes. *J Exp Med.* 2007;204(6):1371-1381.
16. Winrow CJ, Pankratz DG, Vibat CR, et al. Aberrant recombination involving the granzyme locus occurs in Atm−/− T-cell lymphomas. *Hum Mol Genet.* 2005;14(18):2671-2684.
17. Zha S, Bassing CH, Sanda T, et al. ATM-deficient thymic lymphoma is associated with aberrant tcrd rearrangement and gene amplification. *J Exp Med.* 2010;207(7):1369-1380.
18. Rothenberg EV, Moore JE, Yui MA. Launching the T-cell-lineage developmental programme. *Nat Rev Immunol.* 2008;8(1):9-21.
19. Taghon T, Yui MA, Pant R, Diamond RA, Rothenberg EV. Developmental and molecular characterization of emerging beta- and gammadelta-selected pre-T cells in the adult mouse thymus. *Immunity.* 2006;24(1):53-64.
20. Herzog KH, Chong MJ, Kapsetaki M, Morgan JI, McKinnon PJ. Requirement for Atm in ionizing radiation-induced cell death in the developing central nervous system. *Science.* 1998;280(5366):1089-1091.
21. Wang X, Xiao G, Zhang Y, et al. Regulation of Tcrb recombination ordering by c-Fos-dependent RAG deposition. *Nat Immunol.* 2008;9(7):794-801.
22. David-Fung ES, Yui MA, Morales M, et al. Progression of regulatory gene expression states in fetal and adult pro-T-cell development. *Immunol Rev.* 2006;209:212-236.
23. Tydell CC, David-Fung ES, Moore JE, Rowen L, Taghon T, Rothenberg EV. Molecular dissection of prethymic progenitor entry into the T lymphocyte developmental pathway. *J Immunol.* 2007;179(1):421-438.
24. Anderson MK, Hernandez-Hoyos G, Dionne CJ, Arias AM, Chen D, Rothenberg EV. Definition of regulatory network elements for T cell development by perturbation analysis with PU.1 and GATA-3. *Dev Biol.* 2002;246(1):103-121.
25. Schmitt TM, Zuniga-Pflucker JC. Induction of T cell development from hematopoietic progenitor cells by delta-like-1 in vitro. *Immunity.* 2002;17(6):749-756.
26. Ito K, Hirao A, Arai F, et al. Regulation of oxidative stress by ATM is required for self-renewal of haematopoietic stem cells. *Nature.* 2004;431(7011):997-1002.
27. Ito K, Takubo K, Arai F, et al. Regulation of reactive oxygen species by Atm is essential for proper response to DNA double-strand breaks in lymphocytes. *J Immunol.* 2007;178(1):103-110.
28. Carbonari M, Cherchi M, Paganelli R, et al. Relative increase of T cells expressing the gamma/delta rather than the alpha/beta receptor in ataxia-telangiectasia. *N Engl J Med.* 1990;322(2):73-76.
29. Levelt CN, Mombaerts P, Iglesias A, Tonegawa S, Eichmann K. Restoration of early thymocyte differentiation in T-cell receptor beta-chain-deficient mutant mice by transmembrane signaling through CD3 epsilon. *Proc Natl Acad Sci U S A.* 1993;90(23):11401-11405.
30. Bagley J, Cortes ML, Breakefield XO, Iacomini J. Bone marrow transplantation restores immune system function and prevents lymphoma in Atm-deficient mice. *Blood.* 2004;104(2):572-578.
31. Janas ML, Varano G, Gudmundsson K, Noda M, Nagasawa T, Turner M. Thymic development beyond beta-selection requires phosphatidylinositol 3-kinase activation by CXCR4. *J Exp Med.* 2010;207(1):247-261.
32. Trampont PC, Tosello-Trampont AC, Shen Y, et al. CXCR4 acts as a costimulator during thymic beta-selection. *Nat Immunol.* 2010;11(2):162-170.
33. Liang HE, Hsu LY, Cado D, Cowell LG, Kelsoe G, Schlissel MS. The "dispensable" portion of RAG2 is necessary for efficient V-to-DJ rearrangement during B and T cell development. *Immunity.* 2002;17(5):639-651.
34. Taylor AM, Metcalfe JA, Thick J, Mak YF. Leukemia and lymphoma in ataxia telangiectasia. *Blood.* 1996;87(2):423-438.
35. Liyanage M, Weaver Z, Barlow C, et al. Abnormal rearrangement within the alpha/delta T-cell receptor locus in lymphomas from Atm-deficient mice. *Blood.* 2000;96(5):1940-1946.
36. Callén E, Jankovic M, Difilippantonio S, et al. ATM prevents the persistence and propagation of chromosome breaks in lymphocytes. *Cell.* 2007;130(1):63-75.
37. Deriano L, Chaumeil J, Coussens M, et al. The RAG2 C terminus suppresses genomic instability and lymphomagenesis. *Nature.* 2011;471(7336):119-123.
38. Ikawa T, Hirose S, Masuda K, et al. An essential developmental checkpoint for production of the T cell lineage. *Science.* 2010;329(5987):93-96.
39. Dujka ME, Puebla-Osorio N, Tavana O, Sang M, Zhu C. ATM and p53 are essential in the cell-cycle containment of DNA breaks during V(D)J recombination in vivo. *Oncogene.* 2010;29(7):957-965.
40. Bednarski JJ, Nickless A, Bhattacharya D, Amin RH, Schlissel MS, Sleckman BP. RAG-induced DNA double-strand breaks signal through Pim2 to promote pre-B cell survival and limit proliferation. *J Exp Med.* 2012;209(1):11-17.
41. Stanulla M, Wang J, Chervinsky DS, Thandla S, Aplan PD. DNA cleavage within the MLL breakpoint cluster region is a specific event which occurs as part of higher-order chromatin fragmentation during the initial stages of apoptosis. *Mol Cell Biol.* 1997;17(7):4070-4079.
42. Betti CJ, Villalobos MJ, Diaz MO, Vaughan AT. Apoptotic stimuli initiate MLL-AF9 translocations that are transcribed in cells capable of division. *Cancer Res.* 2003;63(6):1377-1381.
43. Yang C, Tang X, Guo X, et al. Aurora-B mediated ATM serine 1403 phosphorylation is required for mitotic ATM activation and the spindle checkpoint. *Mol Cell.* 2011;44(4):597-608.
44. Li M, Fang X, Baker DJ, et al. The ATM-p53 pathway suppresses aneuploidy-induced tumorigenesis. *Proc Natl Acad Sci U S A.* 2010;107(32):14188-14193.
45. Nakamura K, Du L, Tunuguntla R, et al. Functional characterization and targeted correction of ATM mutations identified in Japanese patients with ataxia-telangiectasia. *Hum Mutat.* 2012;33(1):198-208.
46. Aifantis I, Raetz E, Buonamici S. Molecular pathogenesis of T-cell leukaemia and lymphoma. *Nat Rev Immunol.* 2008;8(5):380-390.

Cancer Cell
Article

An Inv(16)(p13.3q24.3)-Encoded *CBFA2T3-GLIS2* Fusion Protein Defines an Aggressive Subtype of Pediatric Acute Megakaryoblastic Leukemia

Tanja A. Gruber,[1,6,8] Amanda Larson Gedman,[6] Jinghui Zhang,[2,8] Cary S. Koss,[1] Suresh Marada,[3] Huy Q. Ta,[6] Shann-Ching Chen,[7] Xiaoping Su,[2,25] Stacey K. Ogden,[3] Jinjun Dang,[6] Gang Wu,[2] Vedant Gupta,[1] Anna K. Andersson,[6] Stanley Pounds,[5] Lei Shi,[5] John Easton,[8] Michael I. Barbato,[8] Heather L. Mulder,[8] Jayanthi Manne,[8] Jianmin Wang,[4,8] Michael Rusch,[2,8] Swati Ranade,[24] Ramapriya Ganti,[6] Matthew Parker,[2] Jing Ma,[7] Ina Radtke,[6] Li Ding,[8,11] Giovanni Cazzaniga,[13] Andrea Biondi,[14] Steven M. Kornblau,[9] Farhad Ravandi,[10] Hagop Kantarjian,[10] Stephen D. Nimer,[15] Konstanze Döhner,[16] Hartmut Döhner,[16] Timothy J. Ley,[8,11,12] Paola Ballerini,[17] Sheila Shurtleff,[6] Daisuke Tomizawa,[20] Souichi Adachi,[21] Yasuhide Hayashi,[22] Akio Tawa,[23] Lee-Yung Shih,[18] Der-Cherng Liang,[19] Jeffrey E. Rubnitz,[1] Ching-Hon Pui,[1] Elaine R. Mardis,[8,11,12] Richard K. Wilson,[8,11,12] and James R. Downing[6,8,*]

[1]Department of Oncology
[2]Department of Computational Biology
[3]Department of Biochemistry
[4]Information Sciences
[5]Department of Biostatistics
[6]Department of Pathology
[7]Hartwell Center for Biotechnology and Bioinformatics
[8]St. Jude Children's Research Hospital, Washington University Pediatric Cancer Genome Project
St. Jude Children's Research Hospital, Memphis, TN 38105, USA
[9]Department of Blood and Marrow Transplantation
[10]Department of Leukemia
University of Texas MD Anderson Cancer Center, Houston, TX 77030, USA
[11]The Genome Institute at Washington University
[12]Siteman Cancer Center
Washington University School of Medicine, St. Louis, MO 63110, USA
[13]Centro Ricerca Tettamanti, Pediatric Clinic, University of Milan-Bicocca, 20052 Monza, Italy
[14]Pediatric Unit, University of Milan-Bicocca, San Gerardo Hospital, 20900 Monza, Italy
[15]Molecular Pharmacology and Chemistry Program, Sloan Kettering Institute, New York, NY 10065, USA
[16]Department of Internal Medicine III, University of Ulm, 89081 Ulm, Germany
[17]Laboratoire d'Hématologie, Hôpital A. Trousseau, 75012 Paris, France
[18]Division of Hematology-Oncology, Department of Internal Medicine, Chang Gung Memorial Hospital, Chang Gung University, Taipei 105, Taiwan
[19]Division of Pediatric Hematology Oncology, Mackay Memorial Hospital, Taipei 104, Taiwan
[20]Department of Pediatrics, Tokyo Medical and Dental University, Tokyo 113-8510, Japan
[21]Human Health Sciences, Graduate School of Medicine, Kyoto University, Kyoto 606-8501, Japan
[22]Department of Haematology/Oncology, Gunma Children's Medical Center, Shibukawa 377-8577, Japan
[23]Department of Pediatrics, National Hospital Organization Osaka National Hospital, Osaka 540-0006, Japan
[24]Pacific Biosciences, Menlo Park, CA 94025, USA
[25]Present address: Department of Bioinformatics and Computational Biology, University of Texas MD Anderson Cancer Center, Houston, TX 77030, USA
*Correspondence: james.downing@stjude.org
http://dx.doi.org/10.1016/j.ccr.2012.10.007

SUMMARY

To define the mutation spectrum in non-Down syndrome acute megakaryoblastic leukemia (non-DS-AMKL), we performed transcriptome sequencing on diagnostic blasts from 14 pediatric patients and validated our

Significance

Acute megakaryoblastic leukemia (AMKL) accounts for 10% of childhood acute myeloid leukemia (AML). Although AMKL patients with Down syndrome (DS-AMKL) have an excellent survival, non-DS-AMKL patients have an extremely poor outcome with a 3 year survival of less than 40%. With the exception of the t(1;22) seen in the majority of infants with non-DS-AMKL, little is known about the molecular lesions that underlie this leukemia subtype. Our results identified a fusion gene, *CBFA2T3-GLIS2*, that functions as a driver mutation in a subset of these patients. Importantly, pediatric patients with *CBFA2T3-GLIS2* expressing AMKL had inferior outcomes (5 year survival 34.3% versus 88.9%; p = 0.03), demonstrating that this lesion is a prognostic factor in this leukemia population.

findings in a recurrency/validation cohort consisting of 34 pediatric and 28 adult AMKL samples. Our analysis identified a cryptic chromosome 16 inversion (inv(16)(p13.3q24.3)) in 27% of pediatric cases, which encodes a CBFA2T3-GLIS2 fusion protein. Expression of CBFA2T3-GLIS2 in *Drosophila* and murine hematopoietic cells induced bone morphogenic protein (BMP) signaling and resulted in a marked increase in the self-renewal capacity of hematopoietic progenitors. These data suggest that expression of CBFA2T3-GLIS2 directly contributes to leukemogenesis.

INTRODUCTION

Acute megakaryoblastic leukemia (AMKL) accounts for approximately 10% of pediatric acute myeloid leukemia (AML) and 1% of adult AML (Athale et al., 2001; Barnard et al., 2007; Oki et al., 2006; Tallman et al., 2000). AMKL is divided into two subgroups: AMKL arising in patients with Down syndrome (DS-AMKL), and leukemia arising in patients without Down syndrome (non-DS-AMKL). Although DS-AMKL patients have an excellent prognosis with an ~80% survival, non-DS-AMKL patients do not fare as well, with a reported survival of only 14%–34% despite high-intensity chemotherapy (Athale et al., 2001; Barnard et al., 2007; Creutzig et al., 2005). With the exception of the t(1;22) seen in infant non-DS-AMKL, little is known about the molecular lesions that underlie this leukemia subtype (Carroll et al., 1991; Lion et al., 1992; Ma et al., 2001; Mercher et al., 2001).

We recently reported data from a high-resolution study of DNA copy number abnormalities (CNAs) and loss of heterozygosity on pediatric de novo AML (Radtke et al., 2009). These analyses demonstrated a very low burden of genomic alterations in all pediatric AML subtypes except AMKL. AMKL cases were characterized by complex chromosomal rearrangements and a high number of CNAs. To define the functional consequences of the identified chromosomal rearrangements in non-DS-AMKL, the St. Jude Children's Research Hospital-Washington University Pediatric Cancer Genome Project performed transcriptome and exome sequencing on diagnostic leukemia samples.

RESULTS

AMKL Is Characterized by Chimeric Transcripts

Transcriptome sequencing was performed on diagnostic leukemia cells from 14 pediatric non-DS-AMKL patients (discovery cohort) (see Tables S1 and S2 available online). Our analysis identified structural variations (SVs) that resulted in the expression of chimeric transcripts encoding fusion proteins in 12 of 14 cases (Table S3). Remarkably, in 7 of 14 cases, a cryptic inversion on chromosome 16 (inv(16)(p13.3q24.3)) was detected that resulted in the joining of *CBFA2T3*, a member of the ETO family of nuclear corepressors, to *GLIS2*, a member of the GLI family of transcription factors (Figures 1, 2, and S1). In six of these cases, exon 10 of *CBFA2T3* was fused to exon 3 of *GLIS2*, whereas in the remaining one case, exon 11 of *CBFA2T3* was fused to exon 1 of *GLIS2*. Both encoded proteins retain the three CBFA2T3 N-terminal *nervy* homology regions that mediate protein interactions and the five GLIS2 C-terminal zinc finger domains that bind the *Glis* DNA consensus sequence (Figures 1A and 1B). Whole-genome sequence analysis of tumor and germline DNA from four cases demonstrated that the *CBFA2T3-GLIS2* chimeric gene resulted from simple balanced inversions in three cases and a complex rearrangement involving chromosomes 16 and 9 in the fourth case (Figures 2 and S1).

Chimeric transcripts were also detected in five of seven leukemia samples that lacked expression of *CBFA2T3-GLIS2*, including one case each expressing in-frame fusions of *GATA2-HOXA9*, *MN1-FLI1*, *NIPBL-HOXB9*, *NUP98-KDM5A*, *GRB10-SDK1*, and *C8orf76-HOXA11AS* (Figure 3; Table S3). Importantly, several of the genes involved in these translocations play a direct role in normal megakaryocytic differentiation (*GATA2* and *FLI1*), have been previously shown to be involved in leukemogenesis (*HOXA9*, *MN1*, *HOXB9*, *NUP98*, *KDM5A*), or are highly expressed in hematopoietic stem cells or myeloid/megakaryocytic progenitors (Figure S2) (Argiropoulos and Humphries, 2007; Buijs et al., 2000; Heuser et al., 2011; Kawada et al., 2001; Visvader et al., 1995; Wang et al., 2009). Analysis of a recurrency/validation cohort consisting of diagnostic leukemia cells from 62 AMKL cases (34 pediatric and 28 adult) revealed 6 additional pediatric samples carrying *CBFA2T3-GLIS2* for an overall frequency of 27% (13 of 48) in pediatric AMKL (Table S1). None of the adult AMKL cases contained this chimeric transcript, suggesting that this lesion is restricted to pediatric non-DS-AMKLs. *NUP98-KDM5A* was the only other chimeric transcript that was recurrent, being detected in 8.3% (4 of 48) of pediatric cases (Table S1). This chimeric transcript was also not detected in adult AMKLs.

Cooperating Lesions in AMKL

In addition to the described chimeric transcripts, exome sequence analysis on 10 of the 14 samples in the discovery cohort that had matched germline DNA, coupled with CNAs detected by Affymetrix SNP6 microarrays, revealed an average of 5 (range 1–14) somatic nonsilent sequence mutations and 5 (range 0–11) CNAs involving annotated genes per case. (Tables S4, S5, and S6; Figure S1). Despite the relative paucity of somatic mutations, recurrent lesions were identified in *JAK* kinase genes, *MPL* and *GATA1*, which have been previously shown to play a role in AMKL (Malinge et al., 2008). Sequence analysis of these genes in cases within the recurrency cohort that had available genomic DNA revealed activating mutations in *JAK* kinases (9 of 51, 17.6%) and *MPL* (2 of 51, 3.9%), as well as inactivating mutations in *GATA1* (5 of 51, 9.8%) (Tables S1 and S6). In addition, 7 of 14 cases with available copy number data contained amplification of chromosome 21 in the Down syndrome critical region (DSCR; chr21q22) that includes genes known to play a role in AML such as *RUNX1*, *ETS2*, and *ERG* (Table S4; Figure S1). Three of these cases carry the *CBFA2T3-GLIS2* chimeric gene. Importantly, the total burden of somatic mutations was significantly lower in the *CBFA2T3-GLIS2*-expressing cases (7.17 ± 3.60 versus 16.60 ± 5.13; $p = 0.009$; Table S5).

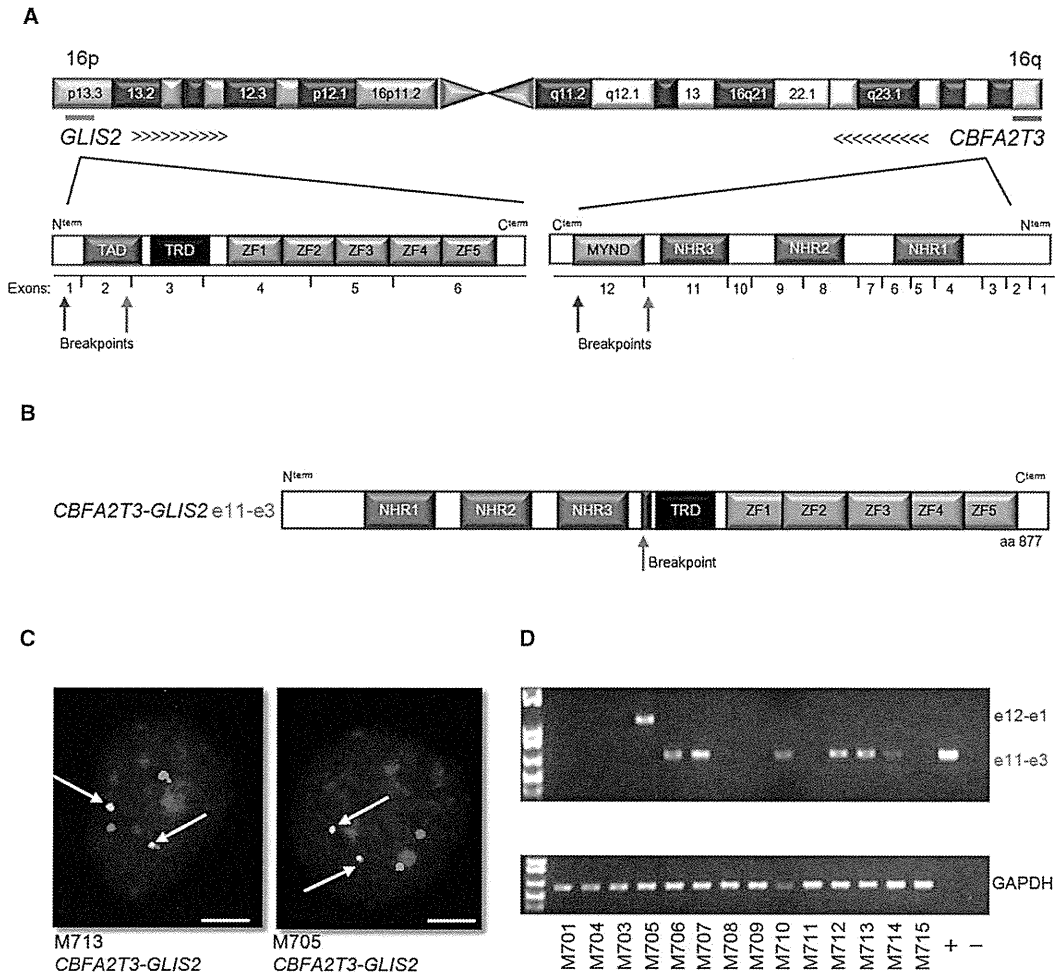

Figure 1. Inv(16)(p13.3;q24.3) Encodes a *CBFA2T3-GLIS2* Chimeric Transcript

(A) Schematic of chromosome 16 with locations of *GLIS2* and *CBFA2T3* shown. Arrows indicate orientation of the gene and the green and red lines the probes used for FISH. The protein structure of the genes is shown below chromosome 16 and is not drawn to scale. Breakpoints are indicated by arrows. TAD, transactivation domain; TRD, transcriptional regulatory domain; ZF, zinc finger; NHR, nervy homology region.

(B) Schematic of CBFA2T3-GLIS2 chimeric protein.

(C) Interphase FISH analysis of two representative patient samples carrying *CBFA2T3-GLIS2*. The *GLIS2* probe is green; the *CBFA2T3* probe is red. White arrows indicate the fusion event. Scale bars, 10 μm.

(D) RT-PCR for CBFA2T3-GLIS2 and GAPDH on the discovery cohort.

See also Figure S1 and Tables S1, S2, S3, S4, S5, and S6.

CBFA2T3-GLIS2 AMKL Is a Distinct Subtype of Pediatric AMKL with a Poor Prognosis

The gene expression profile of *CBFA2T3-GLIS2* AMKL was distinct from that of AMKL cells lacking this chimeric transcript and from other genetic subtypes of pediatric AML (Figures 4A and 4B). A detailed coexpression network analysis of the top 4,000 differentially expressed genes suggests that expression of *CBFA2T3-GLIS2* leads to marked upregulation of *BMP2*, a downstream target of Hedgehog signaling (Figures 4B and S3; Table S7). Moreover, gene set enrichment analysis based on KEGG pathway annotation of the top-scoring network module demonstrated Hedgehog and JAK-STAT pathways to be significantly upregulated in *CBFA2T3-GLIS2*-positive AMKL (Figure S3).

Given the historically poor outcomes seen in pediatric non-DS-AMKL, we next explored whether the presence of *CBFA2T3-GLIS2* identified a clinically distinct subset of cases. Outcome data were available on 40 pediatric patients. Although these patients were treated at a number of different centers using a variety of different therapeutic approaches, the presence of *CBFA2T3-GLIS2* identified a subgroup of patients with a significantly worse overall survival at 5 years as compared to patients with AMKL that lacked this chimeric transcript (28.1% versus 41.9%; p = 0.05; Figure 4C). Moreover, when this analysis was limited to patients treated at a single institution (St. Jude, n = 19), the adverse prognostic impact of *CBFA2T3-GLIS2* on survival was maintained (34.3% versus 88.9%; p = 0.03; Figure 4D).

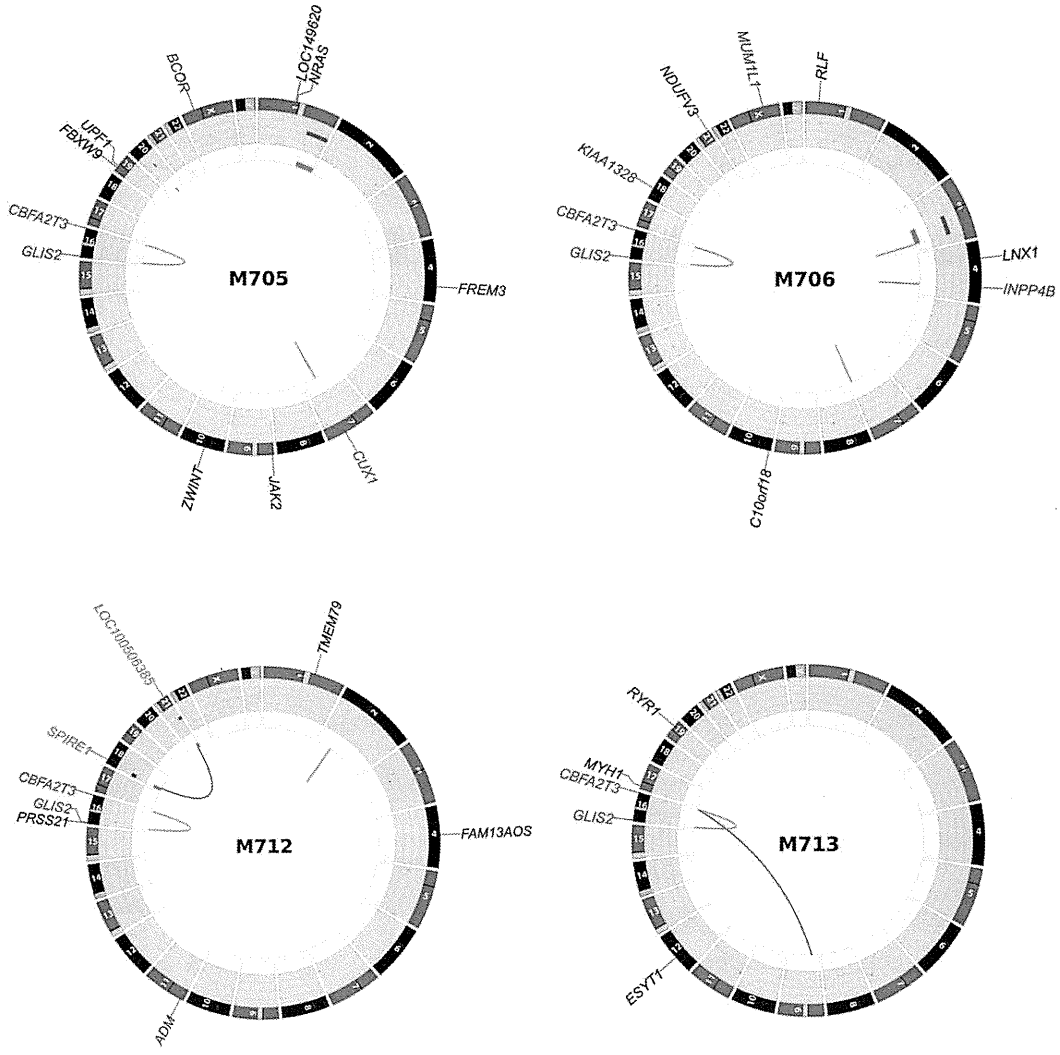

Figure 2. Somatic Mutations in Whole-Genome-Sequenced AMKL Cases

Plots depict structural genetic variants, including DNA copy number alterations, intra- and interchromosomal translocations, and sequence alterations (Krzywinski et al., 2009). DNA copy number alterations: loss of heterozygosity (LOH), orange; amplification, red; deletion, blue. Sequence mutations in Refseq genes: silent SNVs (SNVs), black; UTR, brown; nonsilent SNVs, blue. Genes at structural variant breakpoints: genes involved in in-frame fusions, red; others, green.

CBFA2T3-GLIS2-Modified Hematopoietic Cells Demonstrate Enhanced Self-Renewal

CBFA2T3 (also known as *MTG16*) was initially identified as a fusion partner with *RUNX1* in rare cases of therapy-related AML that contain a t(16;21)(q24;q22) (Gamou et al., 1998). More recently, CBFA2T3 has been implicated in the maintenance of hematopoietic stem cell quiescence (Chyla et al., 2008). By contrast, to our knowledge, GLIS2 has not been previously implicated in leukemogenesis. GLIS2 is a member of the GLI-similar (GLIS1-3) subfamily of Krüppel-like zinc finger transcription factors and is closely related to the GLI family of transcription factors that function as critical elements of the hedgehog signaling pathway (Kim et al., 2007; Lamar et al., 2001). GLIS2 is expressed in the kidney, and germline-inactivating mutations lead to nephronophthisis, an autosomal recessive cystic kidney disease (Attanasio et al., 2007). Although *GLIS2* is not normally expressed in the hematopoietic system, its fusion to *CBFA2T3* as a result of the inv(16)(p13.3q24.3) results in high-level expression of the C-terminal portion of the protein including its DNA-binding domain (Figure S1).

To explore the functional effects of the CBFA2T3-GLIS2 fusion protein, we transduced murine hematopoietic cells with a retrovirus expressing either *CBFA2T3-GLIS2* or *GLIS2* alone and assessed their effect on in vitro colony formation, differentiation, and replating efficiency as a surrogate measure of self-renewal (Figures 5A and 5B). On the initial plating, the expression of CBFA2T3-GLIS2 had no effect on colony numbers, size, or overall myeloid/erythroid differentiation when cells were grown in the presence of IL3, IL6, SCF, and EPO. However, hematopoietic cells transduced with the empty

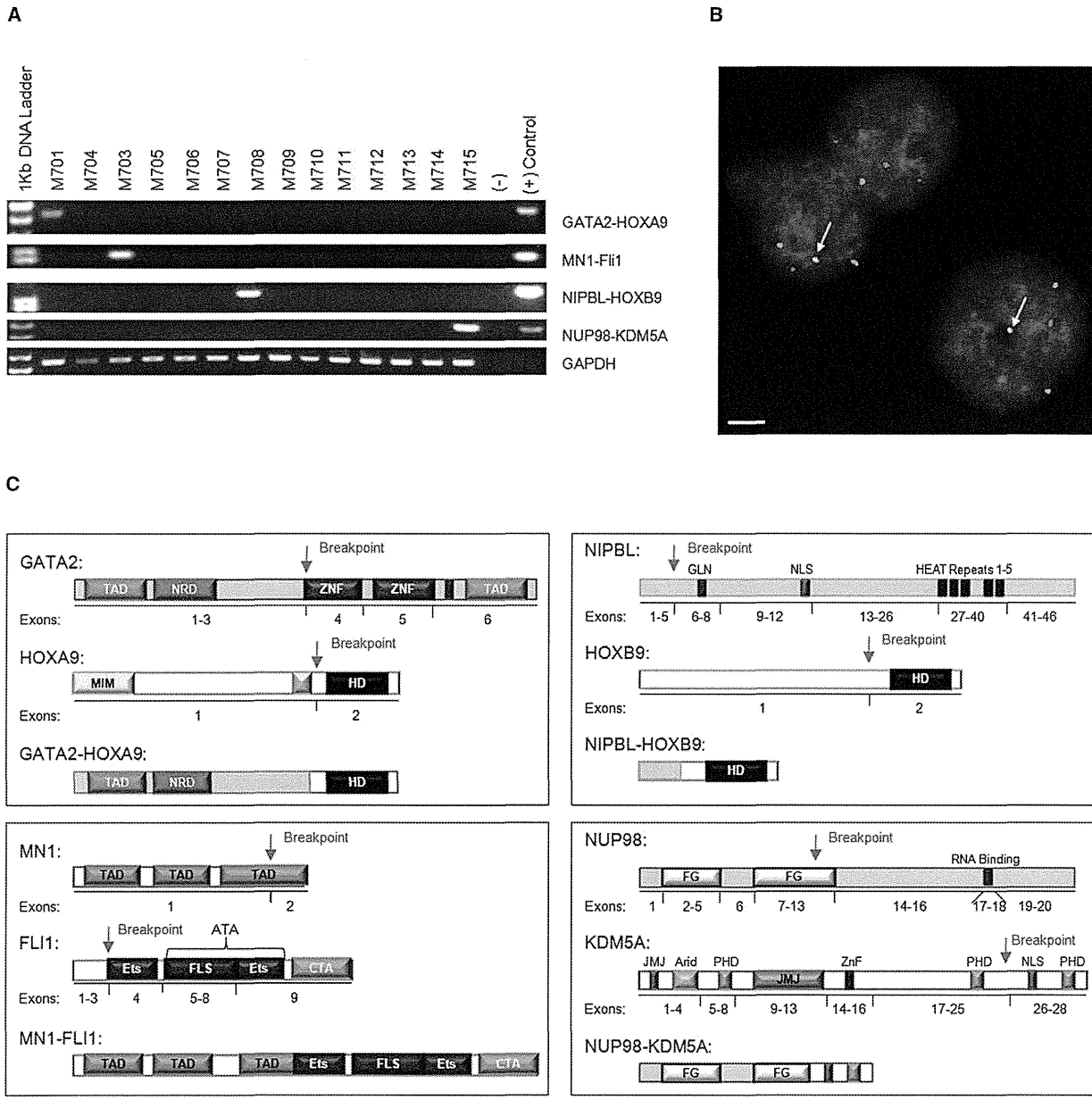

Figure 3. Low-Frequency Chimeric Transcripts in Pediatric AMKL

Four chimeric transcripts were identified in one case each of the discovery cohort and tested for in the recurrency cohort: *GATA2-HOXA9*, *MN1-FLI1*, *NIPBL-HOXB9*, and *NUP98-KDM5A*.

(A) RT-PCR validation of the discovery cohort. Primers and conditions are described in Supplemental Experimental Procedures.

(B) Interphase FISH analysis of M703 carrying the MN1-FLI1 chimeric protein. The *MN1* probe is red; the *FLI1* probe is green. White arrows indicate the fusion event. Scale bar, 10 μm.

(C) Schematic of chimeric proteins. Exons and domains are not drawn to scale. NRD, negative regulatory domain; ZNF, zinc finger; MIM, Meis interaction motif; HD, Hox domain; Ets, E-twenty six domain; FLS, Fli1-specific region; CTA, C-terminal transactivation domain; GLN, glutamine-rich domain; NLS, nuclear-localizing signal; HEAT, *H*untingtin/*E*F3/PP2A/*T*OR1 domain; FG, phenylalanine-glycine repeats; JMJ, jumonji domain; ARID, AT-rich interaction domain; PHD, plant homeodomain. See also Figure S2.

retrovirus (MSCV-IRES-mCherry [MIC]) failed to form colonies after the second replating, whereas expression of either CBFA2T3-GLIS2 or wild-type GLIS2 resulted in a marked increase in the self-renewal capacity, with colony formation persisting through ten replatings (Figure 5C). Upon serial replating, two colony types were detected: CFU-GM and CFU-Meg

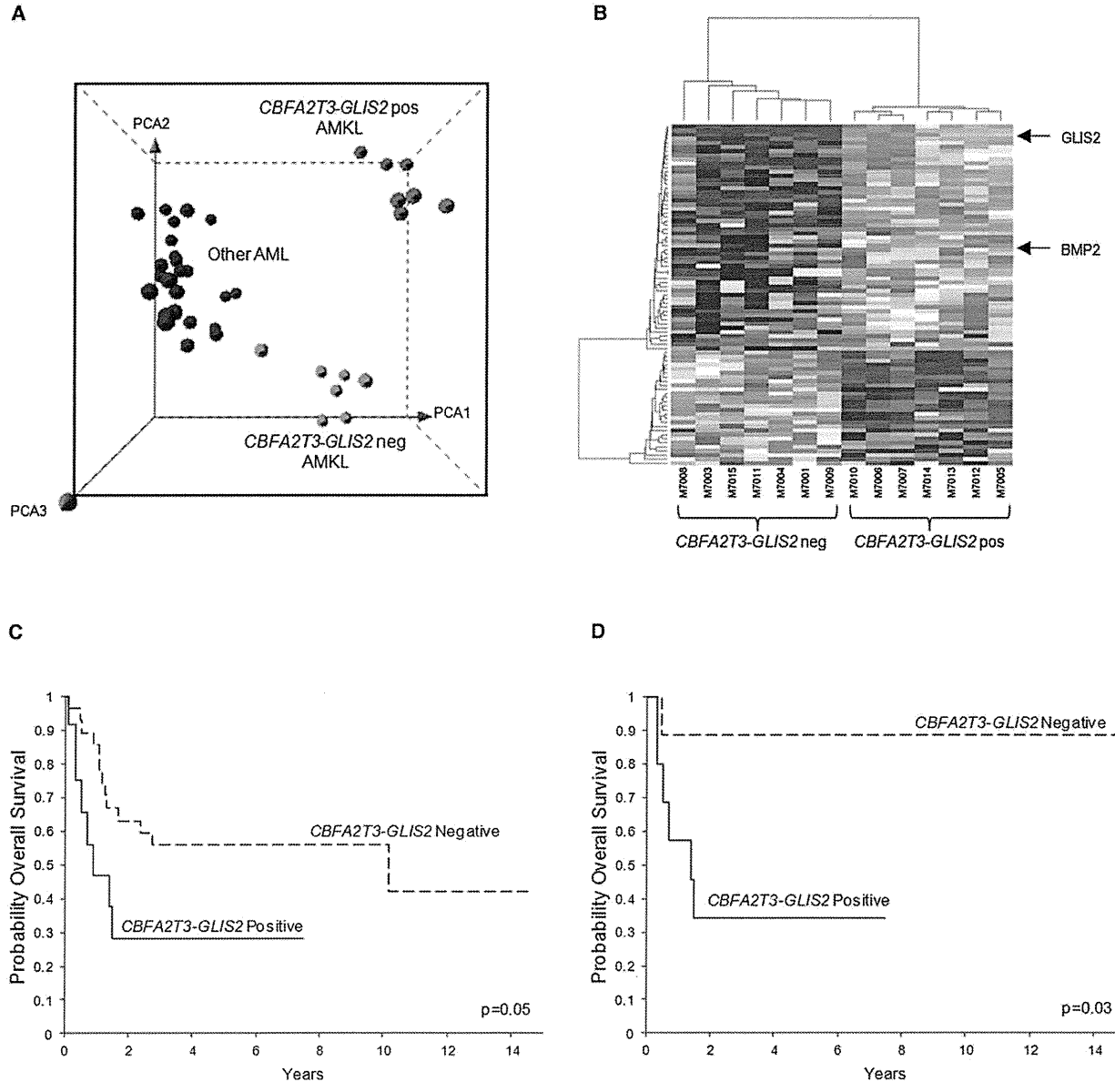

Figure 4. *CBFA2T3-GLIS2* Defines a Unique Subtype of AML with a Distinct Gene Expression Signature and Poor Outcomes

(A) Principal component analysis of the gene expression profiles of the AMKL discovery cohort and 32 other non-AMKL AML samples representing all other known genetic subtypes of pediatric AML. Clusters were generated using 1,000 genes selected by k-means algorithm. A detailed description of the samples included in this analysis can be found at NCBI Gene Expression Omnibus, accession GSE35203.

(B) Heatmap of differentially expressed genes in the top-scoring network module of CBFA2T3-GLIS2-positive (pos) and -negative (neg) AMKL patient samples. For gene relationships, please see Figure S3. For a detailed list of the top 500 differentially expressed genes (not limited to this network), please see Table S7.

(C) Overall survival of 40 pediatric non-DS AMKL cases treated at multiple institutions (*CBFA2T3-GLIS2*-negative cases n = 28, and *CBFA2T3-GLIS2*-expressing cases, n = 12). The curves for the two groups were tested by log rank method and exact test using permutation that yielded a p value of 0.05.

(D) Overall survival of 19 pediatric non-DS AMKL cases treated at St. Jude Children's Research Hospital (*CBFA2T3-GLIS2*-negative cases, n = 9, and *CBFA2T3-GLIS2*-expressing cases, n = 10). The curves for the two groups were tested by log rank method and exact test using permutation that yielded a p value of 0.03. See also Figure S3 and Table S7.

(Figure 5D). Immunophenotypic analysis at the third replating also revealed evidence of megakaryocytic differentiation with CD41/CD61 dual expression and the absence of cKIT and Sca1 expression in the majority of cells (Figure 5E). Importantly, CBFA2T3-GLIS2-expressing cells remained growth factor dependent, suggesting that cooperating mutations in growth factor

signaling pathways are likely required for full leukemic transformation (data not shown). Moreover, transplantation of *CBFA2T3-GLIS2*-transduced bone marrow cells into syngeneic recipients failed to induce overt leukemia at day 365 as demonstrated by normal blood counts and low-level reporter gene expression in peripheral blood (<5%) (data not shown), consistent with a requirement for cooperative mutations. Failure to induce leukemia in mice as a single lesion has been previously reported for other chimeric genes that confer the ability to serially replate in colony-forming assays, including *AML1-ETO* (Higuchi et al., 2002).

CBFA2T3-GLIS2 Induces BMP Signaling

GLIS2 can function as both a transcriptional activator and repressor depending on the cellular context and has been implicated in altered signaling through a number of pathways including sonic hedgehog-GLI1 (SHH) and WNT/β-catenin (Attanasio et al., 2007; Kim et al., 2007). Analysis of the gene expression signatures of *CBFA2T3-GLIS2* expressing AMKLs revealed altered expression of a number of genes in the SHH and WNT pathways, as well as genes in the bone morphogenic protein (BMP) pathway, which is directly influenced by SHH signaling (Figures 4B, 6A, and S3) (Dahn and Fallon, 2000; Ingham and McMahon, 2001; Vokes et al., 2007). When this analysis was limited to genes containing GLI consensus DNA-binding sites (Gli-BS) in their promoters or to genes known to be transcriptional targets of GLIS2, marked overexpression of *PTCH1*, *HHIP*, *BMP2*, and *BMP4* was observed (Figures 6B, S3, and S4; Table S7) (Attanasio et al., 2007). Consistent with this observation, although CBFA2T3-GLIS2 only weakly activated transcription of a reporter construct containing the Gli-BS (Figure S4), it strongly activated transcription of the Gli-BS-containing BMP4 promoter-driven luciferase construct and induced expression of BMP4 in murine hematopoietic cells (Figures 6C and S4). Moreover, CBFA2T3-GLIS2 strongly activated a BMP response element (BRE) containing luciferase reporter construct and induced expression of the BMP downstream transcriptional target, inhibitor of differentiation 1 (*ID1*) (Korchynskyi and ten Dijke, 2002), consistent with the induced expression of BMP2/BMP4 (Figure S4).

BMP signaling plays a critical role in the specification of hematopoiesis in developing embryos, and studies suggest that BMP4 stimulation can augment megakaryocytic output from CD34 progenitors (Jeanpierre et al., 2008; Söderberg et al., 2009). To determine if the observed CBFA2T3-GLIS2-induced BMP expression contributes to the enhanced replating capacity of murine hematopoietic cells, colony-replating assays were repeated in the presence of dorsomorphin, a selective small molecule inhibitor of the BMP type I receptors that blocks BMP-mediated phosphorylation of SMAD 1/5/8 (Yu et al., 2008). Importantly, CBFA2T3-GLIS2 as well as GLIS2-expressing hematopoietic cells were significantly more sensitive to dorsomorphin than wild-type cells in the first plating (Figure 6D). Continuous exposure to dorsomorphin inhibited colony formation in a dose-dependent manner on subsequent platings (data not shown). Interestingly, sublethal doses of dorsomorphin in *CBFA2T3-GLIS2*-positive cells led to an upregulation of *Bmp4* and *Id1* transcripts over time, with colony counts returning to untreated levels, suggesting that cells are able to overcome this inhibition by upregulating the BMP pathway (data not shown).

To further explore the downstream signaling of CBFA2T3-GLIS2 in human leukemia cell lines, we first assessed the expression level of *GLIS2* in human cancer cell lines using the recently published Broad-Novartis Cancer Cell Line Encyclopedia (Figure 7A) (Barretina et al., 2012). Interestingly, this analysis showed that GLIS2 expression levels are lowest in leukemia cell lines. Moreover, within the leukemias, the highest expressing cell line was the pediatric AMKL cell line M07e. To further explore AMKL cell lines, we performed RT-PCR for *CBFA2T3-GLIS2* on five human AMKL cell lines. Three of the five cell lines (RS1, WSU-AML, and M07e) expressed *CBFA2T3-GLIS2* (Figure 7B). The presence of the chimeric gene in these lines was validated by FISH analysis (Figure 7B). We went on to determine the relative expression of BMP genes by semiquantitative RT-PCR and found a trend toward upregulation of these genes in the CBFA2T3-GLIS2-positive cells (Figure 7C). We also assessed our AMKL cell lines for dorsomorphin sensitivity and found a trend toward increased sensitivity in cell lines expressing *CBFA2T3-GLIS2* as determined by a standard MTT assay (Figure 7D).

To determine if CBFA2T3-GLIS2 induces the upregulation of BMP signaling in vivo, we generated transgenic *Drosophila* expressing either *CBFA2T3-GLIS2* or full-length *GLIS2* using an epithelial promoter and examined their effect on fly development. During *Drosophila* development, the WNT, BMP, and SHH homologs (Wg, Dpp, and Hh, respectively) have distinct roles in patterning adult wing structures (Dahn and Fallon, 2000; Ingham and McMahon, 2001; Vokes et al., 2007). When altered, these signaling pathways trigger characteristic loss- and gain-of-function phenotypes (Tabata and Takei, 2004). Expression of CBFA2T3-GLIS2 and full-length GLIS2 in *Drosophila* resulted in ectopic expression of endogenous *dpp*, the fly homolog of *BMP4*, in wing imaginal discs (Figures 8A and S5). Immunofluorescence confirmed the nuclear localization of CBFA2T3-GLIS2 (Figure 8A). Both CBFA2T3-GLIS2 and GLIS2 overexpression induced lethality. However, a small number of escapers developed to pharate adults and demonstrated a morphologic *dpp* gain-of-function phenotype; wing hinges were converted to notum, and legs were shortened and broadened (Figure 8B) (Grieder et al., 2009). Rare *CBFA2T3-GLIS2* transgenic flies developed to adulthood and demonstrated mild ectopic venation throughout the wing blade, as well as wing blistering consistent with a *dpp* gain-of-function phenotype (Figure 8B) (Sander et al., 2010).

DISCUSSION

Sequence analysis of pediatric non-DS-AMKLs revealed the expression of an inv(16)-encoded *CBFA2T3-GLIS2* in almost 30% of pediatric non-DS-AMKL patients, and its presence defined a distinct subgroup of patients that had an exceptionally poor outcome when compared to patients with AMKL that lacked this lesion. In addition, five other chimeric transcripts (*GATA2-HOXA9*, *MN1-FLI1*, *NIPBL-HOXB9*, *GRB10-SDK1*, and *C8orf76-HOXA11AS*) were detected in single AMKL cases. Surprisingly, none of the identified chimeric transcripts was detected in adult AMKL cases, highlighting the significant

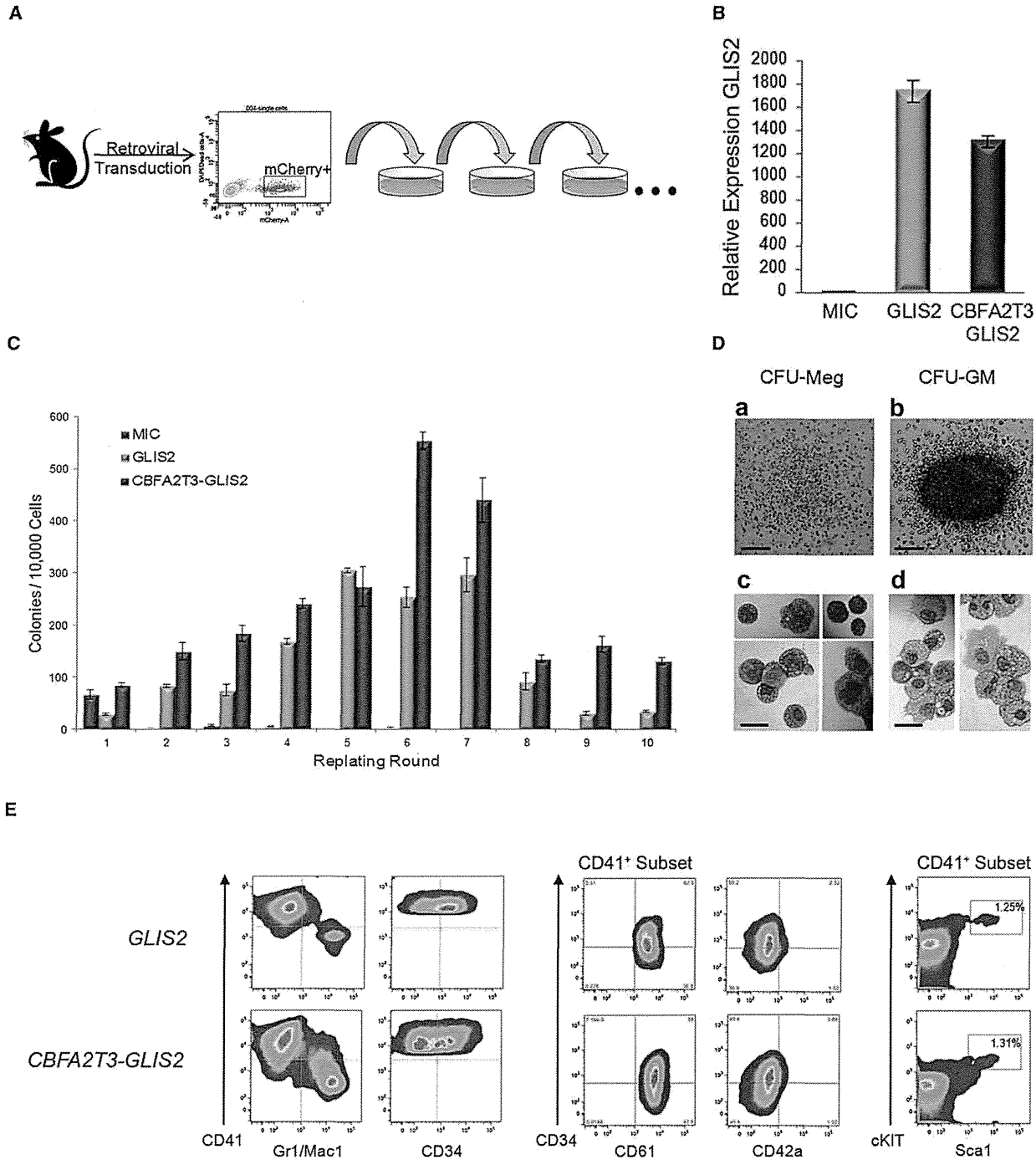

Figure 5. *CBFA2T3-GLIS2* Leads to Enhanced Replating of Hematopoietic Cells

(A) Experimental design. Murine bone marrow cells were transduced with retroviral vectors expressing mCherry alone (MIC), or mCherry along with *GLIS2*, or *CBFA2T3-GLIS2*. Transduced cells were purified by sorting mCherry-positive cells and plated onto methylcellulose containing IL3, IL6, SCF, and EPO. Colonies were counted after 7 days of growth and replated serially.

(B) Semiquantitative RT-PCR of GLIS2 utilizing cells harvested from first round of plating. *GLIS2* primers are specific for the 3′ half of the transcript and thus pick up both full-length GLIS2 as well as CBFA2T3-GLIS2. Expression in MIC cells was defined as one (1), and data are pooled from two separate experiments with similar results. $p \leq 0.0001$ as determined by one-way ANOVA. Error bars represent mean ± SEM of two independent experiments.

(C) Number of colonies detected at 7 days following each plating. Error bars represent mean ± SEM of two independent experiments.

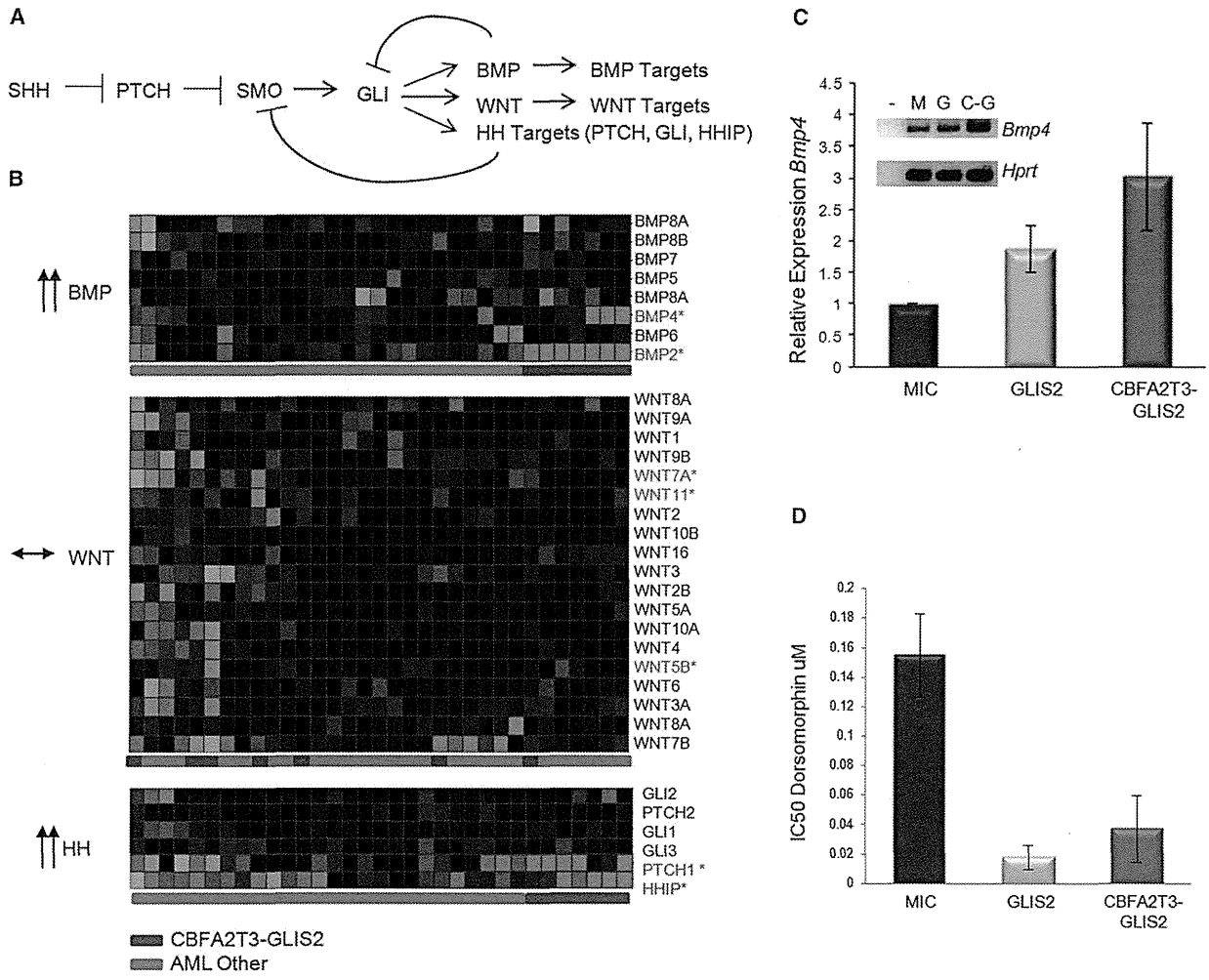

Figure 6. *CBFA2T3-GLIS2* Activates the BMP Pathway

(A) The Hedgehog (HH) signaling pathway. In addition to classic hedgehog targets such as *PTCH* and *HHIP*, *WNT* and *BMP* gene expression have been demonstrated to be affected by the GLI transcription factor in various models (Dahn and Fallon, 2000; Ingham and McMahon, 2001; Vokes et al., 2007).

(B) Gene expression profiles from *CBFA2T3-GLIS2* containing AMKL cases and other AML subtypes were evaluated for expression levels of *BMP*, *WNT*, and HH target genes. *CBFA2T3-GLIS2*-negative AMKL cases are not shown in this analysis. Significantly upregulated probe sets (FDR less than 0.05) are designated with red font: BMP2 FDR 1.06 × 10–17, BMP4 FDR 0.015976, PTCH1 FDR 2.05 × 10–6, and HHIP FDR 0.0038.

(C) Murine bone marrow cells were transduced with retroviral vectors carrying mCherry alone (MIC), mCherry plus *GLIS2*, or *CBFA2T3-GLIS2*. mCherry-positive cells were sorted and plated in methylcellulose containing IL3, IL6, SCF, and EPO. Following 1 week of growth, RNA was isolated, reverse transcribed, and amplified with *Bmp4* or *Hprt*-specific primers. Error bars represent mean ± SEM of four independent experiments. A representative gel is shown (–, neg; M, MIC; G, *GLIS2*; C-G, *CBFA2T3-GLIS2*). p = 0.047 as determined by one-way ANOVA.

(D) *GLIS2* and *CBFA2T3-GLIS2* sensitize murine hematopoietic cells to BMP receptor type I inhibition. Colony-formation assays were conducted in the presence or absence of dorsomorphin at the indicated concentrations (Yu et al., 2008). IC_{50} values were calculated as the amount of drug required to inhibit 50% of the colony formation as determined by colony counts. Error bars represent mean ± SEM of two independent experiments. p = 0.036 as determined by one-way ANOVA. See also Figure S4.

biological differences between pediatric and adult AMKL. Importantly, each of the detected chimeric transcripts is predicted to encode a fusion protein that would alter signaling pathways known to play a role in normal hematopoiesis, suggesting that these lesions are "driver" mutations that directly contribute to the development of leukemia. In addition to these somatic

(D) Colony morphology detected in *GLIS2* and *CBFA2T3-GLIS2*-modified cells from the second plating and beyond. a, CFU-Meg; b, CFU-GM. Scale bars, 500 μm. Representative cytospins and morphology of each colony type are shown. c, CFU-Meg; d, CFU-GM. Scale bars, 50 μm.

(E) Cells harvested from colony-forming assays after three or more replatings were subjected to flow cytometry. Cells were negative for acetylcholinesterase (data not shown).

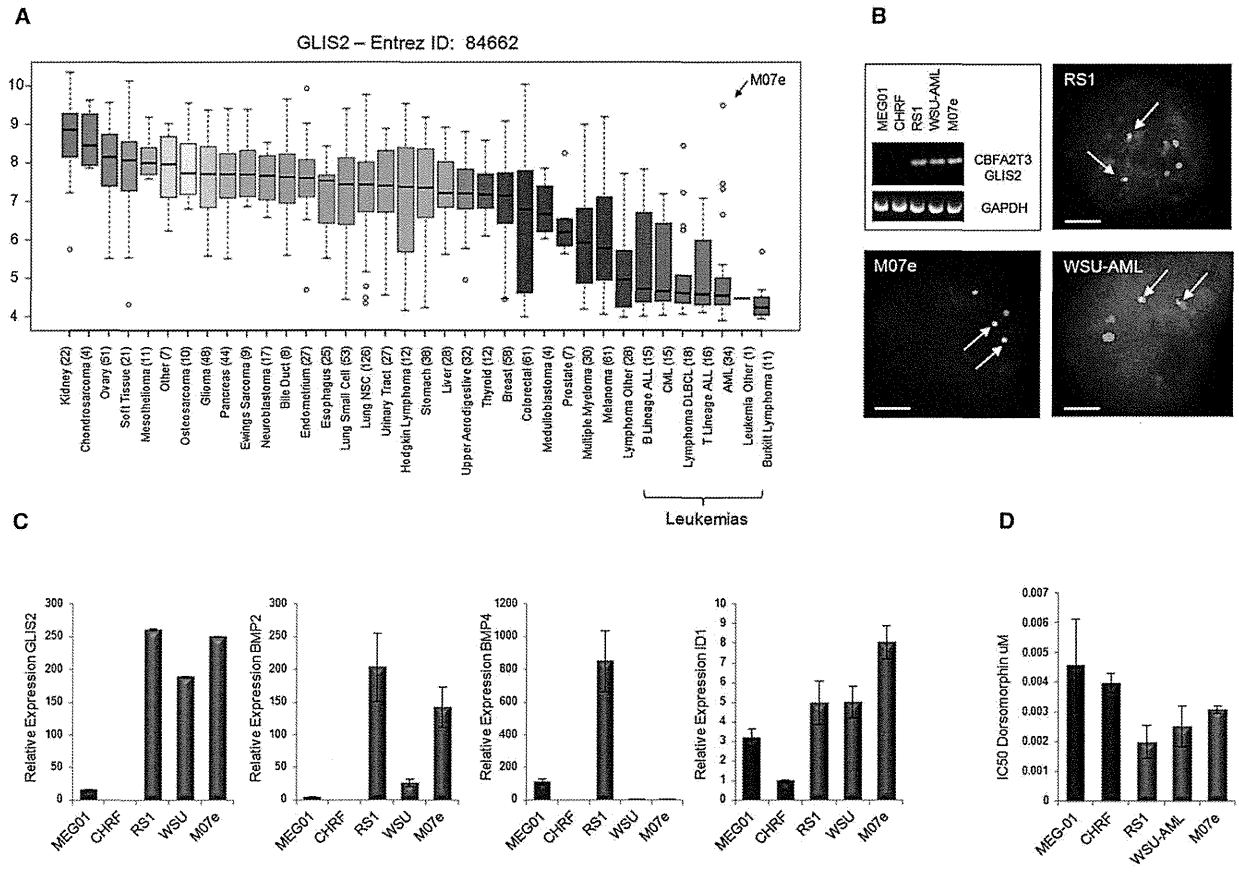

Figure 7. *CBFA2T3-GLIS2* Is Present in AMKL Cell Lines

(A) *GLIS2* expression as determined by gene expression arrays in 991 human cancer cell lines. Log_2-transformed expression levels are shown. Data were obtained from the Broad-Novartis Cancer Cell Line Encyclopedia (http://www.broadinstitute.org/ccle/home). A total of 34 AML cell lines are included; the extreme outlier of this subtype, M07e, is indicated. The *GLIS2* probe set recognizes the end of the transcript and thus does not distinguish between wild-type *GLIS2* and *CBFA2T3-GLIS2*. Median values are indicated by the band within the box plots; the ends of the whiskers indicate upper and lower adjacent values. Outliers are denoted by open circles.

(B) RT-PCR on five AMKL cell lines: MEG-01, CHRF-288-11, RS-1, WSU-AML, and M07e. The three cell lines carrying *CBFA2T3-GLIS2* were validated by FISH. Scale bars, 10 μm.

(C) Real-time semiquantitative RT-PCR of *GLIS2*, *BMP2*, *BMP4*, and *ID1* on the five AMKL cell lines. Expression levels relative to β-actin are shown. CHRF-288-11 expression levels were set to one (1) for comparison across cell lines. Error bars represent mean ± SEM of two independent experiments.

(D) Dorsomorphin sensitivity in the cell lines as determined by MTT assay. Error bars represent mean ± SEM of two independent experiments. For cell line information and MTT assay, please see Supplemental Experimental Procedures.

structural alterations, a variety of other somatic mutations were detected, including activating mutations in kinase signaling pathways in 21.6% of cases (*JAK* kinase family members and *MPL*), inactivating mutations in *GATA1* in 9.8% of cases, and amplification of chromosome 21 in the DSCR that includes genes known to play a role in AML such as *RUNX1*, *ETS2*, and *ERG* in 50% of the cases. How these mutations interact to not only induce overt leukemia but also to influence therapeutic responses remains to be determined.

As part of the St. Jude Children's Research Hospital-Washington University Pediatric Cancer Genome Project, we have sequenced 260 cases of pediatric cancers across multiple tumor types (Downing et al., 2012). The CBFA2T3-GLIS2 fusion was limited to AMKL cases. This specificity may exist for several reasons. The N-terminal portion of the fusion, CBFA2T3, is primarily expressed in the hematopoietic compartment, leading one to predict that expression of the inversion product, if it were to occur, would primarily be limited to hematopoietic cells. Although we do not know the exact target cell of transformation, induction of BMP4 signaling in human CD34+ progenitors has been demonstrated to increase the percentage of megakaryocyte and erythroid colonies in vitro (Fuchs et al., 2002; Jeanpierre et al., 2008). Thus, enhanced BMP signaling as a result of the expression of the inv(16)-encoded CBFA2T3-GLIS2 may directly contribute to the megakaryocytic differentiation of the leukemia cells.

The inv(16)-encoded *CBFA2T3-GLIS2* chimeric gene induced aberrant high-level expression of the DNA-binding domain of

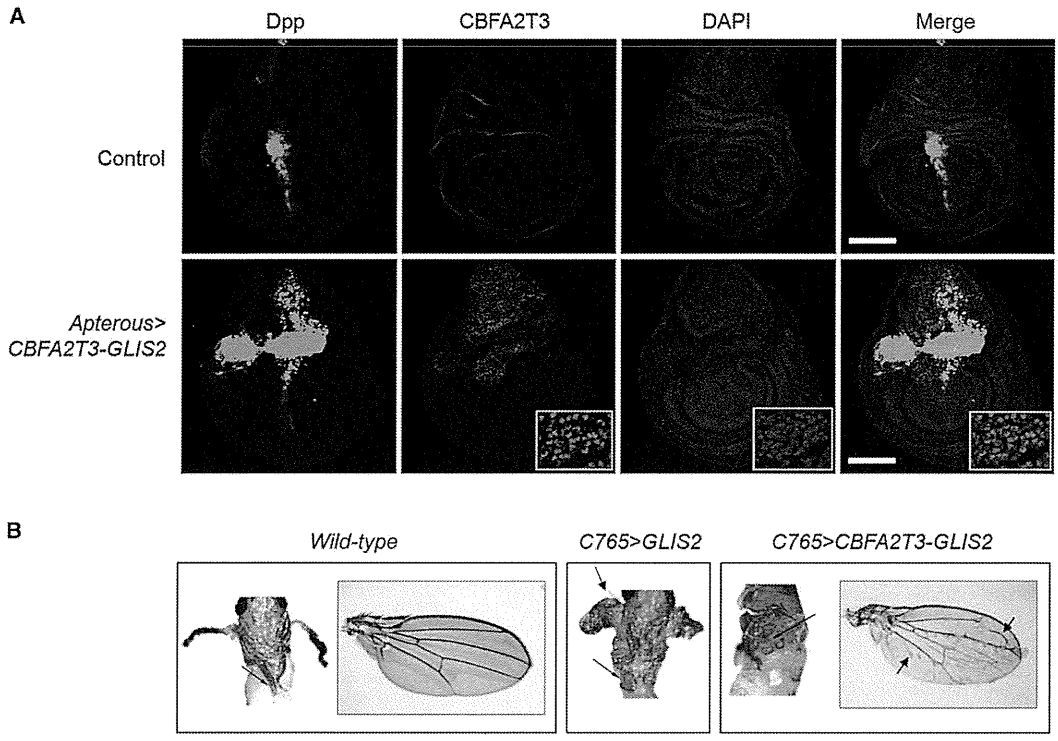

Figure 8. Transgenic *CBFA2T3-GLIS2 Drosophila* Ectopically Expresses Dpp

(A) *CBFA2T3-GLIS2* was expressed under control of *Apterous-Gal4* (strong epithelial dorsal driver). *dpp-lacZ* serves as a reporter for *dpp* induction. Wing imaginal discs were isolated at the late third instar, stained for β-gal as a readout for dpp (green), CBFA2T3 (red), and DAPI (blue), followed by immunofluorescence analysis. Nuclear localization of CBFA2T3-GLIS2 can be seen by the pink signal (inset). Scale bars, 100 μm.

(B) *CBFA2T3-GLIS2* was expressed under control of C765, a weak epithelial driver. Pharate adults were dissected from pupal casings and imaged. Arrows indicate ectopic notum, broadened and shortened legs. No *C765 > GLIS2 Drosophila* matured to adulthood. Arrows indicate ectopic veins in wings of rare *C765 > CBFA2T3-GLIS2* escapers.

See also Figure S5.

GLIS2 in hematopoietic cells, along with the disruption of one allele of *CBFA2T3*, a gene whose encoded protein has been shown to play a role in maintaining normal hematopoietic stem cell quiescence (Chyla et al., 2008). GLIS2 is a distant member of the GLI superfamily of transcriptional factors that function as critical transcriptional targets of the SHH signaling pathway (Hui and Angers, 2011). Although alterations in the SHH pathway have been directly implicated in a range of cancers (Barakat et al., 2010), the role of SHH signaling in normal hematopoiesis and leukemia remains poorly defined (Lim and Matsui, 2010). Our data suggest that aberrant expression of GLIS2 results in upregulation of the classic SHH-negative feedback inhibitors PTCH and HHIP, coupled with a marked increase in the expression of BMP 2 and 4, resulting in enhanced BMP signaling. These results indicate that CBFA2T3-GLIS2 functions, in part, as a gain-of-function GLIS2 allele. The exact mechanisms by which GLIS2 induced the upregulation of BMP2/BMP4 remains incompletely defined, although our data suggest that a direct transcription effect of GLIS2 on the BMP4 promoter is likely, although an indirect mechanism may also contribute.

Interestingly, BMP4 has been shown to expand and maintain human cord blood hematopoietic stem cells in vitro both directly, as well as indirectly via SHH signaling (Bhardwaj et al., 2001; Bhatia et al., 1999). Furthermore, *ID1*, a downstream BMP target previously implicated in leukemogenesis, was found to be upregulated in *CBFA2T3-GLIS2*-modified hematopoietic cells, demonstrating that this pathway is activated (Wang et al., 2011). Consistent with these findings, we demonstrated that activation of BMP signaling contributed to the marked increase in the replating capacity of myeloid/erythroid-committed progenitors. Accordingly, we found that murine hematopoietic cells carrying either full-length *GLIS2*, or *CBFA2T3-GLIS2*, demonstrated an increased sensitivity to BMP inhibition, suggesting that upregulation of this pathway contributes to the observed phenotype. In addition, BMP4 signaling has been shown to induce the differentiation of human CD34+ progenitors into megakaryocytes (Jeanpierre et al., 2008), suggesting that the upregulation of this pathway is also contributing to the megakaryocyte differentiation phenotype of these leukemias. Finally, BMP4, like thrombopoietin, appears to exert its effects on human megakaryopoiesis in part through the JAK/STAT pathways (Jeanpierre et al., 2008). Interestingly, functional pathway analysis of gene expression profiles in *CBFA2T3-GLIS2*-positive AMKL samples identified genes in the Jak-STAT signaling pathway to be significantly upregulated ($p = 0.0038$; FDR 0.022978; Figure S4). Combined with the identification in some cases of

activating mutations in either JAK family members or MPL in *CBFA2T3-GLIS2*-expressing leukemias, our data suggest that these lesions likely cooperate in leukemogenesis.

Taken together, these data define a poor prognostic subgroup of pediatric AMKL patients that are characterized by the inv(16)(p13.3q24.3)-encoded CBFA2T3-GLIS2 fusion protein. Expression of *CBFA2T3-GLIS2* induces an enhanced replating capacity of lineage-committed myeloid progenitors, along with megakaryocytic differentiation, in part through enhanced BMP2/BMP4 signaling. Whether altered SHH and CBFA2T3-induced signaling also contributes to leukemogenesis remains to be determined. Nevertheless, the presented data raise the important possibility that inhibition of the BMP pathway may have a therapeutic benefit in this aggressive form of pediatric AML.

EXPERIMENTAL PROCEDURES

Patients and Samples

Paired-end transcriptome sequencing on diagnostic leukemic blasts was performed on 14 pediatric non-DS-AMKL cases using the Illumina platform. Four of these cases underwent whole-genome sequencing (WGS) on diagnostic leukemia blasts and matched germline samples. All 14 cases underwent whole-exome sequencing for which 10 had matching germline samples. One additional diagnostic sample with matched germline DNA had whole-exome sequencing done that did not undergo transcriptome sequencing. All 15 of these patients were treated at St Jude Children's Research Hospital from 1990 to 2008. The recurrence cohort consisted of 61 additional cases including 33 pediatric specimens and 28 adult specimens . All samples were obtained with patient or parent/guardian-provided informed consent under protocols approved by the Institutional Review Board at each institution and St. Jude Children's Research Hospital.

Sequencing

RNA and DNA library construction for transcriptome and whole-genome DNA sequencing, respectively, has been described previously (Mardis et al., 2009; Zhang et al., 2012). Analysis of WGS data and whole-exome sequencing data that include mapping, coverage and quality assessment, single-nucleotide variant (SNV)/Indel detection, tier annotation for sequence mutations, prediction of deleterious effects of missense mutations, and identification of loss of heterozygosity was described previously (Zhang et al., 2012). Please see Supplemental Experimental Procedures for details.

Recurrency Screening for Sequence Variations and Fusions

We performed recurrence screening on a cohort of 61 AMKL samples. All 61 were screened by RT-PCR (see Supplemental Experimental Procedures for primers and conditions) for *CBFA2T3-GLIS2*, *GATA2-HOXA9*, *MN1-FLI1*, *NIPBL-HOXB9*, and *NUP98-KDM5A*. Whole-genome-amplified DNA (QIAGEN) from 38 cases underwent PCR and Sanger sequencing by Beckman Coulter Genomics for *JAK1*, *JAK2*, *JAK3*, and *MPL* mutations. In 8 of 38 cases, a paired matched germline was available. Putative SNVs and indel variants were detected by SNPdetector (Zhang et al., 2005).

Overall Survival Probabilities

Outcome data were available for 40 pediatric patients tested for *CBFA2T3-GLIS2*. *CBFA2T3-GLIS2* was found in 13 patients. Overall survival was defined as the date of diagnosis or study enrollment to the date of death with surviving patients censored at the date of last follow-up. Survival curves were estimated using the Kaplan-Meier method and compared using the exact log rank test based on 10,000 permutations.

Affymetrix SNP Array

Affymetrix SNP 6.0 array genotyping was performed for 14 of 15 AMKL cases in the discovery cohort, and array normalization and DNA copy number alterations were identified as previously described (Lin et al., 2004; Mullighan et al., 2007; Olshen et al., 2004; Pounds et al., 2009). To differentiate inherited copy number alterations from somatic events in leukemia blasts from patients lacking matched normal DNA, identified putative variants were filtered using public copy number polymorphism databases and a St. Jude database of SNP array data from several hundred samples (Iafrate et al., 2004; McCarroll et al., 2008).

Gene Expression Profiling

Gene expression profiling was performed using Affymetrix Human Exon 1.0 ST Arrays (Affymetrix) according to manufacturer's instructions. This cohort comprised 39 pediatric AML samples including AMKL (n = 14), *AML1-ETO* (n = 4), *CBFB-MYH11* (n = 2), *MLL* rearranged (n = 3), *PML-RARA* (n = 2), *NUP98-NSD1* (n = 2), *HLXB9-ETV6* (n = 1), and AML cases lacking chimeric genes (n = 11). Please see Supplemental Experimental Procedures for further details.

FISH

Dual-color FISH was performed on archived bone marrow cells and cell lines as described previously by Mullighan et al. (2007). Probes were derived from bacterial artificial chromosome (BAC) clones (Invitrogen). BACs used were RP11-830F9 (*CBFA2T3*), CTD-25555M20 (*GLIS2*), RP11-345E21 (*MN1*), and CTD-2542E23 (*FLI1*). BAC clone identity was verified by T7 and SP6 BAC-end sequencing and by hybridization of fluorescently labeled BAC DNA with normal human metaphase preparations.

Cloning of CBFA2T3-GLIS2 and GLIS2

Total RNA was extracted from leukemia blasts using RNeasy (QIAGEN) and reverse transcribed using Superscript III (Invitrogen) as per manufacturer's instructions. The coding region of *CBFA2T3-GLIS2* was PCR amplified from patient M712 and M707 using primers CBFA2T3_119F and GLIS2_1685R (see Supplemental Experimental Procedures for primers and conditions). *GLIS2* was PCR amplified from cDNA using primers GLIS2_21F and GLIS2_1685R (see Supplemental Experimental Procedures for primers and conditions). PCR products were subcloned into the pGEM-T Easy Vector (Promega) and sequenced. Clones containing the correct sequence were then subcloned into the MIC retroviral backbone (Volanakis et al., 2009).

Murine Bone Marrow Transduction and Colony-Forming Assays

All experiments involving mice were reviewed and approved by the Institutional Animal Care and Use Committee. Bone marrow from 4- to 6-week-old female C57/BL6 mice was harvested and cultured in the presence of recombinant murine SCF (rmSCF), IL3 (rmIL3), and IL6 (rmIL6) (Peprotech; all 50 ng/ml) for 24 hr prior to transduction on RetroNectin (Takara Bio)-coated plates. Ecotropic envelope-pseudotyped retroviral supernatant was produced by transient transfection of 293T cells as previously described by Soneoka et al. (1995). Forty-eight hours following transduction, cells were harvested, sorted for mCherry expression, and plated on methylcellulose containing IL3, IL6, SCF, and EPO (Stem Cell Technologies, Vancouver, British Columbia, Canada) as per manufacturer's instructions. Colonies were counted after 7 days of growth at 37°C, harvested, and replated. In a subset of experiments, dorsomorphin (Sigma-Aldrich) was added to the methylcellulose at the indicated concentrations.

Flow Cytometry

Cells were resuspended in PBS and preincubated with anti-CD16/CD32 Fc-block (BD PharMingen) if staining did not include conjugated anti-murine CD16/32. Aliquots were stained for 15 min at 4°C with conjugated antibodies. Cells were washed and resuspended in DAPI containing solution (1 μg/ml DAPI in PBS) for subsequent analysis using FACS LSR II D (BD Biosciences). For a list of antibodies used, please see Supplemental Experimental Procedures.

Luciferase Assays

The human BMP4 promoter-driven luciferase construct pSLA4.1EX (Van den Wijngaard et al., 1999) was kindly provided by E. Joop van Zoelen, Nijmegen, The Netherlands. The murine BMP response element (pBRE) (Korchynskyi and ten Dijke, 2002) was kindly provided by Peter ten Dijke, Leiden, The Netherlands. The 8 × 3′ Gli-BS luciferase reporter (pGli-BS) (Sasaki et al., 1997) has been previously described. TOPFlash and FOPFlash (Korinek et al., 1997) constructs were obtained from Addgene. For details on luciferase reporter assays, please see Supplemental Experimental Procedures.